TOWARDS FABRICATION OF FLEXIBLE SOLAR CELLS USING PN-JUNCTION GAAS NANOWIRES

TOWARDS FABRICATION OF FLEXIBLE SOLAR CELLS USING PN-JUNCTION GAAS NANOWIRES

By

NUZHAT AHMED, B.Sc. (PUNJAB UNIVERSITY, PAKISTAN)

A Thesis

Submitted to the School of Graduate Studies

In Partial Fulfillment of the Requirements

For the Degree

Master of Applied Science

McMaster University

MASTER OF APPLIED SCIENCE (2008) McMaster University

(Engineering Physics) Hamilton, Ontario

TITLE: Towards Fabrication of Flexible Solar cells Using pn-junction GaAs Nanowires

AUTHOR: Nuzhat N. Ahmed, B.Sc. Physics (Punjab University, Pakistan)

SUPERVISOR: Dr. R. R. LaPierre

NUMBER OF PAGES: xiii, 87

Abstract

In the current research, use of p-n junction GaAs nanowires (NWs) grown by gas source molecular beam epitaxy on GaAs (111) B substrates for the fabrication of flexible solar cells are reported. The solar cells were fabricated by embedding the NWs in a polymer matrix (SU8 2), followed by ohmic contact formation to the tops of the NWs as well as the rear side of the substrate. I-V characteristic curves were obtained by illuminating the solar cells using a solar simulator, indicating a photovoltaic effect. NWs were also detached from the substrate by different methods and successfully transferred onto a flexible substrate for potential use as solar cells. Scanning electron microscopy was used throughout the research for characterization and optimization of the fabrication processes including NW embedment, removal from the substrate, and contact formation.

Acknowledgements

I would like to express my sincere appreciation and gratitude to my supervisor Dr. Ray LaPierre for his consistent guidance, technical insight, support and encouragement during the past two years, which made this learning period a rewarding experience for me.

I wish to acknowledge a whole lot of people, my friends, colleagues and the research staff for their help at every step of the way. I would like to extend my thanks to Brad Robinson for making this research possible by GS-MBE growths and for helpful suggestions; Graham Pearson, Doug Bruce, Doris Stevanovic, Zhillin Peng, Peter Jonasson for training to use the different equipment and informative discussions from time to time. I would like to acknowledge the staff of Brockhouse Institute for Materials Research for their assistance in using the SEM facility, especially Steve Koprich for accommodating me with extra time and Glynis De Silveira for her valuable discussions. I would also like to express my deepest gratitude to Martin Plante for sharing his knowledge and friendship with me throughout the two years. I owe many thanks to Shahram Tavakoli, Josef Czaban, Farseem Mohammadi, my friends Nooshin Tajik and Hanna Budz for their time and valuable advice. Many thanks are also due to Chris Hapamaaki, Subir Ghosh, and Parsian Mohseni for their encouraging discussions.

I would love to extend my deepest gratitude to my friends Mihaela Grigore, Charles Mahoney, Vijay Muthukumaru, and Marlene Wachko without whom I would not have been able to start this huge project at this time of my life. I would especially like to thank my friend Tim Griffiths for his continued support before and during these two years.

My acknowledgements would not be complete if I did not mention my friend and cousin Samia Rashad, and my friend Najma and Uncle Ghulam Mohyuddin who helped me in more than one ways during this tough time of study and juggling with other aspects of my life.

Finally, I would like to express my heartfelt appreciation and gratitude to my family: my husband Zahid for his continued love, extra patience, financial support and believing in me at all times; my two kids Raza and Zain for their understanding, love, and patience; my parents, brother and sisters for their unconditional love and good wishes.

Table of Contents

List of Figures

List of Tables

Chapter 1: Physics of Solar Cells

1.1 Motivation Behind Nanowire Solar Cells

The most daunting challenge faced by today's world is to find sufficient supplies of clean energy for the future. This is due to the fact that world demand for energy is projected to more than double by 2050 and to more than triple by the end of the century, and incremental improvements in existing energy networks will not be adequate to supply this demand in a sustainable way. Sunlight provides by far the largest of all carbon neutral, inexhaustible, clean and renewable sources of energy that does not generate greenhouse gases or other harmful pollutants and by-products. More energy strikes the earth in one hour from the sun (4.3×10^{20} J) than all the energy consumed on the planet in one year (4.1×10^{20} J). It is, as such, a compelling solution to our need for clean and abundant source of energy for the future. [1.1]

One way to tame this unlimited supply of energy is by making solar cells that operate by converting sunlight directly into electricity. This challenge is being met head on by researchers all over the world resulting in considerable reduction of cost/watt of delivered solar electricity via photovoltaics. Also, new approaches based on nanostructured architectures are being demonstrated to assist in further reducing the cost of existing photovoltaics, and for improving their efficiency. Nanorods, nanoparticles and nanowires are some of the nanostructures that are being examined for this purpose. [1.2] Of the three, nanowires are receiving special attention in the research world today because of their unique physical properties. They are emerging as a powerful class of materials that,

through controlled growth and organization, have opened up substantial opportunities for use in novel nanoscale solar cells. [1.3]

The electron transport in nanowires is expected to be several orders of magnitude faster than percolation through a random polycrystalline network. As a matter of fact, the direct electrical pathways provided by the nanowires ensure the rapid collection of carriers generated throughout the device. Matt et al.[1.4] in their data analysis on particle injection have reported evidence for faster electron injection in nanowires. Researchers from the University of California, Berkeley led by Peidong Yang[1.5], have reported growing Zn oxide nanowire arrays coated in light absorbing dye instead of nanoparticles and placing them between two electrodes. The nanowires, about 60 nanometers in diameter and 20 micrometers in length conducted electrons from one end of the cell to the other about 100 times more efficiently than other nanoparticle-based solar cells currently under development.

Nanowire heterostructures of III–V materials are of particular interest for their optoelectronic applications. Among the III-Vs, GaAs is becoming the material of choice due to its proven optoelectronic properties. In the current research we report the use of p-n junction GaAs NWs grown by gas source molecular beam epitaxy on GaAs (111) B substrates for the fabrication of flexible solar cells. The solar cells were fabricated by embedding the NWs in a polymer matrix (SU8 2), with the tops of the NWs exposed, followed by ohmic contact formation of the tops of the NWs as well as the rear side of the substrate. I-V characteristic curves were obtained by illuminating the solar cells using a solar simulator, which proved the potential success of this method. NWs were also

detached from the substrate by different methods and successfully transferred onto a flexible substrate for potential use as solar cells. Scanning electron microscopy was used throughout the research for characterization and optimization of the fabrication processes including NW embedment, removal from the substrate, and contact formation.

1.2 Principle of Solar Cells

A constant flux of radiation from the Sun is incident upon the Earth which, with clear sky and dry air, amounts to about 1 kW/m^2. [1.6] A large variety of techniques are available or under development to benefit from this solar energy, including photovoltaic systems, concentrating solar power, passive solar systems, solar hot water, and solar process heat.

Solar cells or photovoltaics (PVs), used to directly convert light energy into electricity, are the most attractive candidates for clean and renewable power.[1.2] They are based on the photovoltaic effect which is the basic physical process allowing conversion of light (photons) into electricity (electrons). In 1839, French physicist Edmund Becquerel discovered the photovoltaic effect while experimenting with an electrolytic cell made of two metal electrodes. He found that certain materials would produce small amounts of electric current when exposed to light. In 1905 Albert Einstein described the nature of light and the photoelectric effect on which the photovoltaic technology is based, but the first ever photovoltaic module was not built until 1954. [1.7]

Solar cells are generally layered structures with an active layer or material sandwiched between two electrodes. The active material needs to be light absorbing and

is usually also semiconducting, meaning that its electrical conductivity is somewhere between that of a metal and that of an insulator. Crystalline solids have a delocalized electronic structure that forms allowed and forbidden energy bands. The energy gap between the top of the highest allowed band that is filled with electrons, the valence band, and the bottom of the lowest allowed band that is empty of electrons, the conduction band, is called the bandgap. The size of the bandgap highly influences the conductivity of a material. Semiconductors have an intermediate bandgap typically in the range of 0.5 to 3 eV. When semiconductors absorb light, the energy of the absorbed photons can be used to excite electrons from the valence band to the conduction band creating electron-hole pairs, so-called excitons. In solar cells, the exciton is then dissociated and the charges (the electrons and holes) are separated and transported to the electrodes to produce a potential difference and eventually a current in an external circuit.

Promotion of electrons in the conduction band occurs if photons with energies equal to or greater than the bandgap are absorbed. Photon energy in excess of the bandgap is usually dissipated as heat and is thus wasted. Alternatively, photons whose energies are less than the bandgap are not absorbed at all but are transmitted through the material. [1.8]

1.3 The p-n Junction in the Dark

There are several different concepts and materials used for making solar cells. The most widely used device structure is the p-n homojunction. A p-n junction is formed when a layer of n-type semiconductor and a layer of p-type material are brought together.

The n-type semiconductor is doped with donor atoms that have more electrons than the surrounding material, and the p-type semiconductor is doped with acceptor atoms that have fewer electrons or positively charged holes, that can move throughout the material and contribute to the current. When a hole and an electron meet, they essentially annihilate each other; this is called recombination.

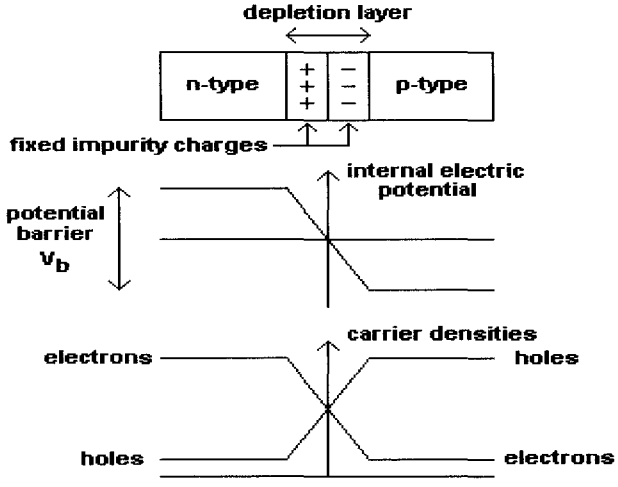

Figure 1.1. The p-n junction in equilibrium. [1.9]

Putting an n-type semiconductor together with a p-type semiconductor creates an electron/hole concentration gradient illustrated in Figure 1.1. This concentration gradient causes diffusion current with electrons diffusing to the p-side and holes diffusing to the n-side. The area in which this diffusion takes place is called the depletion region. When electrons from the n-side diffuse to the p-side they meet with holes and recombine leaving positively charged donor atoms on the n-side. The holes from the p-side diffusing to the n-side create negatively charged acceptor atoms on the p-side. The ionized donors and acceptors create an internal electrostatic field in the depletion region which opposes

any further diffusion across the junction. Only those electrons and holes with a high enough energy to overcome the field can make this transition. Equilibrium is established when diffusion of majority carriers across the junction is balanced by the drift of minority carriers back across the junction in the built-in electric field. At this point the junction region is depleted of charges, the Fermi levels of p- and n-type layers are equal, and the difference in the work functions is taken up by a step in the conduction and valence band edges called the built-in voltage. [1.10]

When a potential is applied across a p-n junction, it can either increase or decrease the internal electric field. If the negative side of the applied potential is connected to the p-side, then the electric field and potential barrier is increased resulting in fewer majority carriers diffusing across the junction so that the net current decreases. This is called a reverse bias (see Figure 1.2).

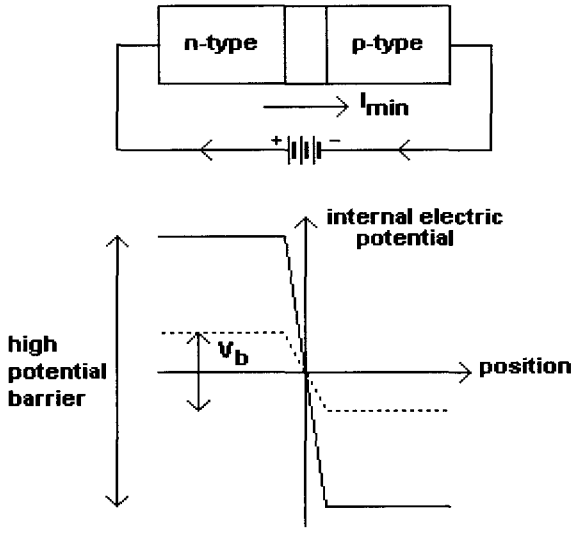

Figure 1.2. Reverse biased p-n junction. [1.9]

Alternately, a forward bias (see Figure 1.3), where the positive side of the potential is connected to the p-side, results in the reduction of the internal field and the potential barrier, enabling more majority carriers to diffuse across the junction so that a net current of electrons from n to p and holes from p to n flows. This is termed injection of the majority carriers.

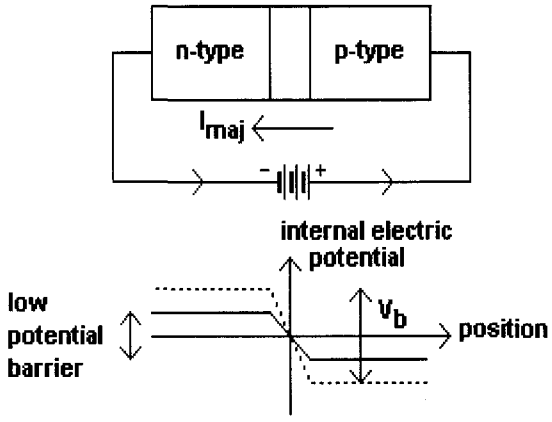

Figure 1.3. Forward biased p-n junction. [1.9]

When the internal field is decreased by a forward bias, the number of electrons on the n-side that have enough energy to cross the depletion region to the p-side increases by a factor of exp(eV/kT) where e is the charge of the electron, V the applied voltage, k the Boltzmann constant, and T the absolute temperature. The resulting electron current I_n from the n-side to the p-side is:

$$I_n = I_{eo} \exp (eV/kT) \qquad \text{Eqn. 1.1}$$

where I_{eo} is the minority electron current flowing from p- to n-side under equilibrium conditions. Thus the total electron current is:

$$I_e = I_{eo} \ [\exp (eV/kT) - 1] \qquad \text{Eqn. 1.2}$$

A forward bias also results in a hole current:

$$I_h = I_{ho} (\exp (eV/kT) - 1) \qquad \text{Eqn. 1.3}$$

where I_{ho} is the equilibrium hole current. Combining Equations 1.2 and 1.3 gives the total current, also known as the diode current:

$$I = I_h + I_e = I_o [\exp(eV/kT) - 1] \qquad \text{Eqn. 1.4}$$

where

$$I_o = I_{ho} + I_{eo} \qquad \text{Eqn. 1.5}$$

is called the dark current. [1.11]

1.4. The p-n Junction under Illumination

When a photon with energy greater than the bandgap is incident on a semiconductor, it gives an electron in the valence band enough energy to move to the conduction band (see Figure 1.4). Both the electron in the conduction band and the hole that has been created in the valence band can be involved in the conduction of a current under an applied electric field.

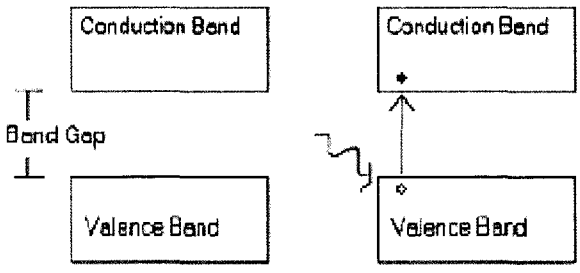

Figure 1.4. Band diagram and electron-hole pair production. [1.12]

A solar cell can be constructed by creating a very thin, heavily doped n-type layer on top of a thicker p-type layer, with both layers usually made of Si. As can be seen in Figure 1.5, the depletion region is mostly on the p-side. Because the n-layer is so thin, most photons penetrate into the depletion region or the p-side before creating an electron-hole pair. When an electron-hole pair is created in the depletion region the electric field moves the electron into the n-side and the hole into the p-side. When a load is connected to the cell, the electron can travel through the circuit, do work, and recombine with the hole from the p-region.

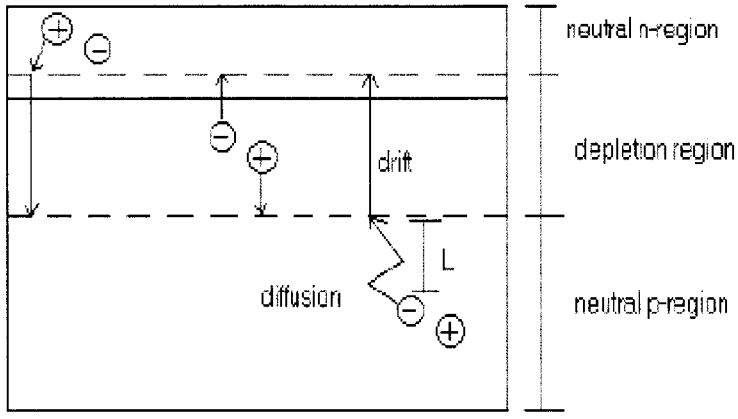

Figure 1.5. Electron-hole pair behavior in a solar cell. [1.12]

If the light penetrates into the neutral p-side, then there is no electric field to separate the electron-hole pair. Instead the electron and the hole diffuse at random through the material and recombine if they meet. The average time between pair production and recombination for an electron is τ_e. In this time, the electron diffuses a mean distance of $L_n = (2D_e\tau_e)^{1/2}$ where D_e is the diffusion coefficient in the p-side.

If the electron-hole pair is created within a diffusion length L_n of the depletion region, then the electron can be moved by the electric field over to the n-side and the hole to the p-side. For this reason it is important for the diffusion length to be as long as possible. The same process takes place for electron-hole pairs created in the n-side. In silicon, the diffusion length is longer for electrons than it is for holes. This is why the thin top region is n-type, and the thicker region is p-type.[1.12] In other words, since $L_p<L_n$, the junction depth must be less than L_p in the n material to allow holes generated near the surfaces to diffuse to the junction before they recombine. Alternately because $L_n>>L_p$, the thickness of the p-region is kept greater than that of the n-region as a compromise in design because the electrons generated in this region can still diffuse to the junction before recombination takes place.

Also another important factor to be considered is reduction of series resistance of the device. It is important that series resistance of the device should be very small so that power is not lost to heat due to ohmic losses in the device itself. A series resistance of only a few ohms can seriously reduce the output power of a solar cell. Keeping the area of the p-region large, the resistance of this part of the device can be made small. It is desirable to have a large contact potential V_o to obtain a large photovoltage and hence heavy doping is indicated. However, long lifetimes are also desirable and these are reduced by doping too heavily.[1.13]

The electric field sweeps the minority carriers to the other side that are generated thermally within a diffusion length of each side of the junction and have diffused to the depletion region. A generation rate g_{op} (electron-hole pairs/cm^3-s) also participates in the

current when the junction is uniformly illuminated by photons with energy greater than the bandgap. The number of electrons created/second within a diffusion length L_n of the transition region on the p side is given by AL_ng_{op} where A is the junction area. Similarly, the number of holes generated/second within a diffusion length L_p of the transition region on the n side is given by AL_pg_{op}. Also, carriers generated within the junction width W is given by AWg_{op}. The resulting current due to collection of these optically generated carriers by the junction is:

$$I_{op} = qAg_{op}(L_p + L_n + W) \qquad \text{Eqn. 1.6}$$

The total reverse current with illumination can be calculated by adding the current I from Eqn. 1.4 and the optical generation current from Eqn. 1.6. Because it is directed from n to p, it can be written as:

$$I = I_o [\exp (eV/kT) - 1] - I_{op} \qquad \text{Eqn. 1.7}$$

This lowers the I-V curve by an amount proportional to the generation rate. The above equation can be considered in two parts, the current due to optical generation and that described by the usual diode equation.

In the case when V = 0 or the device is short-circuited the terms from the diode equation cancel out but the short circuit current from n to p equal to I_{op} exists. Thus the I-V characteristics of the p-n junction cross the I-axis at negative values proportional to g_{op}. On the other hand, when I = 0 at open circuit across the device, $V = V_{oc}$ and is given by:

$$V_{oc} = (kT/e) \ln (I_{op}/I_o + 1) \qquad \text{Eqn. 1.8}$$

This equation shows that V_{oc} increases logarithmically with the light intensity. A solar cell is equivalent to a current generator in parallel with an asymmetric non-linear resistive

element. Under illumination an ideal cell produces a photocurrent proportional to the light intensity. The variable resistance of the diode and the load share this photocurrent in a ratio which depends on the resistance of the load and the level of illumination. There is nothing to drive the photocurrent through the load without the diode.

Equation 1.8 can be written as:

$$V_{oc} \cong (kT/e) \ln(g_{op}/g_{th}) \quad \text{for } g_{op} >> g_{th} \qquad \text{Eqn. 1.9}$$

where g_{th} is the 'equilibrium' thermal generation recombination rate. From the above equation, V_{oc} cannot increase indefinitely with increased generation rate, its limit being the equilibrium contact potential V_o since the lifetime τ_n becomes shorter as the minority carrier concentration, p_n, is increased by optical generation of electron-hole pairs, thus making $g_{th} = p_n/\tau_n$ larger. [1.10]

1.5. I-V Characteristics of a PV Cell

Figure 1.6 shows the current-voltage (I-V) characteristics of a solar cell with and without illumination. Here the shaded portion is the fill factor, defined by:

$$FF = J_m V_m / J_{sc} V_{oc} \qquad \text{Eqn. 1.10}$$

Where J_m and V_m are the current density and the voltage at the maximum power point on the I-V curve, J_{sc} is the short-circuit current, and V_{oc} is the open circuit voltage. [1.14]

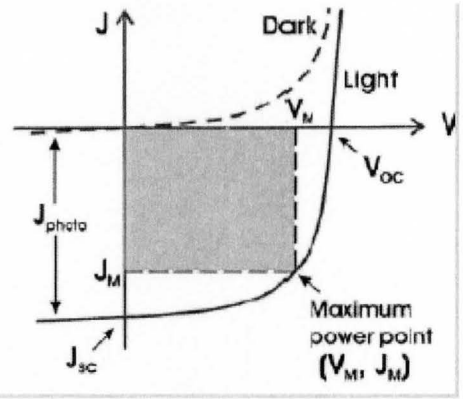

Figure 1.6. Typical I-V curves for a solar cell under illumination and in the dark. [1.14]

A solar cell in a circuit normally generates a dc photovoltage of 0.5 to 1 V and a short circuit photocurrent of some tens of milliamps per cm^2 under standard illumination conditions (1000 W/m^2). The cells are connected together in series or parallel and encapsulated into modules to produce larger output currents or voltages.

The relation between photocurrent density J_{sc} and incident spectrum is given by

$$J_{sc} = \int b_s(E)Q(E)dE \qquad \text{Eqn. 1.11}$$

where $b_s(E)$ is the incident spectral photon flux density and Q(E) is the probability that an incident photon of energy E will deliver one electron to the external circuit. The value of Q(E) is not dependent on the incident spectrum, but on the absorption coefficient of the solar cell material, efficiency of charge separation, and efficiency of charge collection in the device.

At the cell's operating point or maximum power point P reaches a maximum and this occurs at some voltage V_m with a corresponding current I_m and current density J_m. The optimum load thus has sheet resistance given by V_m / J_m or resistance V_m / I_m.

The fill factor (FF) describes the 'squareness' of the I-V curve and is commonly used to collectively describe the degree to which V_m matches V_{oc} and I_m matches I_{sc}. It is defined as shown previously in Equation 1.10, as the ratio:

$$FF = J_m V_m / J_{sc} V_{oc} \qquad \text{Eqn. 1.10}$$

or as:

$$FF = I_m V_m / I_{sc} V_{oc} \qquad \text{Eqn. 1.12}$$

The efficiency η of the cell is the power density at the operating point as a fraction of the incident light power density P_s:

$$\eta = J_m V_m / P_s \qquad \text{Eqn. 1.13}$$

Efficiency is also related to J_{sc} and V_{oc} using FF:

$$\eta = Jsc\ Voc\ FF / P_s \qquad \text{Eqn. 1.14}$$

The four quantities in the above equation: J_{sc}, V_{oc}, FF and η are the key performance characteristics of a solar cell. All of these should be defined for particular illumination conditions. Air Mass 1.5 spectrum, an incident power density of 1000W/m^2 and a temperature of 25°C define the Standard Test Condition (STC) for solar cells. The following table shows the performance characteristics for most common solar cell materials.

Table 1.1. Performance of some types of PV cells. [1.10]

Cell type	Area (cm^2)	V_{oc} (V)	J_{sc} (mA/cm^2)	FF	Efficiency (%)
Crystalline Si	4.0	0.706	42.2	82.8	24.7
Crystalline GaAs	3.9	1.022	28.2	87.1	25.1
Poly-Si	1.1	0.654	38.1	79.5	19.8
a-Si	1.0	0.887	19.4	74.1	12.7
$CuInGaSe_2$	1.0	0.669	35.7	77.0	18.4
CdTe	1.1	0.848	25.9	74.5	16.4

It is evident that the solar cell materials with larger J_{sc} tend to have lower V_{oc}. This is a consequence of the material used and particularly of the bandgap of the semiconductor. Also an important point to note is that there is a fundamental compromise between photocurrent and voltage in photovoltaic energy conversion. [1.10]

1.6. Limitations on Energy Conversion in Solar Cells

In order to improve the efficiency of the solar cell, the emphasis is to maximize absorption, minimize reflection and recombination, and maximize conduction. Much of the energy from sunlight reaching a PV cell is lost before it can be converted into electricity. Carefully designing a PV can improve various characteristics that limit its conversion efficiency.[1.15] Some factors affecting the conversion efficiency are listed below.

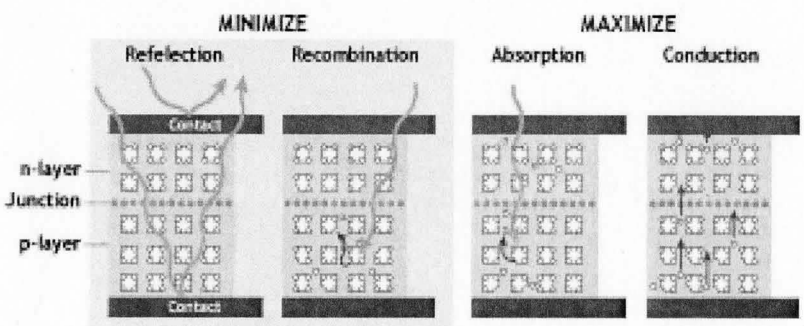

Figure 1.7. Factors affecting efficiency of the solar cell. [1.15]

Wavelength of Light:

Solar cells respond differently to the different wavelengths of light. For example, crystalline silicon can use the entire visible spectrum, plus some part of the infrared spectrum. However, longer wavelength radiation is too low in energy for absorption. Higher energy radiation can produce current flow, but much of this energy is wasted as heat. In summary, light that is too high or low in energy is not usable by a cell to produce electricity. The bandgap, which is the minimum amount of energy needed to free an electron from its bond, differs for different semiconductor materials. The primary reason why PV cells are not 100% efficient is because they cannot respond to the entire spectrum of sunlight. Photons with energy less than the material bandgap are not absorbed, which wastes about 25% of incoming energy in a Si solar cell. The energy content of photons above the bandgap will be wasted surplus—re-emitted as heat or light—and accounts for an additional loss of about 30%. Thus, the inefficient interactions of sunlight with the cell material waste about 55% of the energy from the original sunlight.

Recombination:

Charge carriers, which are electrons and holes, in a solar cell may inadvertently recombine before they make it into the electrical circuit and contribute to the cell's current. Direct recombination is a major problem for some materials, where light-generated electrons and holes randomly encounter each other and recombine. In other materials, indirect recombination occurs, where electrons or holes encounter an impurity,

defect in the crystal structure, or interface or surface that makes it easier for them to recombine.

Natural Resistance:

The natural resistance to electron flow in a cell decreases cell efficiency. These losses predominantly occur in three places: in the bulk of the primary solar material, in the thin top layer typical of many devices, and at the interface between the cell and the electrical contacts leading to an external circuit.

Temperature:

Solar cells work best at low temperatures, as determined by their material properties. All cell materials lose efficiency as the operating temperature rises. Much of the light energy shining on cells becomes heat, so it is beneficial to either match the cell material to the operation temperature or continually cool the cell.

Reflection:

A cell's efficiency can be increased by minimizing the amount of light reflected away from the cell's surface. For example, untreated silicon reflects more than 30% of incident light. Various antireflection (AR) technologies help to optimize light absorption. Most commonly, a special coating is applied to the top layer of the cell. A single AR layer will effectively reduce reflection only at one wavelength. Better results, over a wider range of wavelengths, are possible with multiple AR layers. Another way to reduce

reflection is to texture the top surface of the cell, which causes reflected light to strike a second surface before it can escape, thus increasing the probability of absorption. If the front surface is textured into pyramid shapes for antireflection, all incident light is bent so that it strikes the polished—but otherwise untreated—back surface of the cell at an angle. This texturing causes light to be reflected back and forth within the cell until it is completely absorbed.

Electrical Resistance:

Larger electrical contacts can minimize electrical resistance, but covering a cell with large, opaque metallic contacts would block too much incident light. Therefore, a trade-off must be made between loss due to resistance and loss due to shading effects. Typically, top-surface contacts are designed as grids, with many thin, conductive fingers spread over the cell's surface. Generally, the back-surface contact of a cell is simpler, often being just a layer of metal. Other designs for electrical contacts include placing everything on the cell's back surface, or, as in some thin films, depositing a thin layer of a transparent conducting oxide across the entire cell. [1.15]

Parasitic Resistances:

Power is dissipated in real cells through leakage currents around the sides of the device and resistance of the contacts. These effects can be considered to be equivalent to two parasitic resistances in series (R_s) and in parallel (R_{sh}) with the cell. R_s arises from the resistances of the cell material to current flow, particularly through the front surface

to the contacts and from resistive contacts. Series resistance is a particular problem at high current densities, for instance under concentrated light. The parallel or shunt resistance arises from the leakage of current through the cell around edges of the device and between contacts of different polarity. [1.10]

The fill factor is reduced due to the series and parallel resistances. For an efficient cell we should have R_s as small and R_{sh} as large as possible. The diode equation in the presence of parasitic resistances becomes[1.10]:

$$J = J_{sc} - J_o (\exp q(V + JAR_s)/kT - 1) - (V + JA R_s)/ R_{sh} \qquad \text{Eqn. 1.15}$$

1.7 Concepts for Improving the Efficiency of Solar Cells

In order to utilize the maximum amount of available optical energy it is necessary to design a solar cell with a large area junction located near the surface of the device. Using diffusion or ion implantation for forming the planar junction, the surface has to be coated with appropriate materials to reduce reflection and surface recombination. The junction depth d must be less than L_p in the n material in order to allow the holes generated near the surface to diffuse to the junction before they recombine; similarly the thickness of the p-region must be such that electrons generated in this region can diffuse to the junction before recombination takes place.

A proper match between the electrical diffusion length L_n, the thickness of the p-region and the mean optical penetration depth is required for the above condition to be satisfied. In order to obtain a large photovoltage a large contact potential is required and hence heavy doping is indicated. On the other hand large lifetimes are also advisable but these are reduced by heavy doping.

A very important factor is that the series resistance of the device should be very small and the parallel resistance large so that the power is not lost to heat due to ohmic losses in the device itself. A series resistance of only a few ohms can seriously reduce the output power of a cell. Since the area is large, the resistance of the p-type body of a solar cell can be made small. However the contacts to the thin n-region require special design. If this region is contacted at the edge, current must flow along the thin n-region to the contact resulting in a large series resistance. This can be prevented by distributing the contacts over the n-surface by providing small contact fingers which can serve to reduce the series resistance without appreciably interfering with the incoming light. [1.13]

Reduction of thermalization losses and improvement on the absorption efficiency can be simultaneously achieved by offering the solar cells only photons within a narrow energy interval around the bandgap and processing the other photons by solar cells with a different bandgap. Cells operated in this way are called tandem cells. For the optimal absorbtion of the incident photons the cells are arranged one after the other, optically in series. Electrical contacts between the cells which absorb photons must be avoided which allows only for the connection of the cells electrically in series. Also the voltages of the different cells must have the same sign, which in turn requires that the same type of

membrane of all cells, for example the p-type membrane must face the sun. This means that n-type membrane of the preceding cell is facing the p-type membrane of the following cell.

If the incident solar radiation is focused and concentrated, it can deliver the same power with smaller area of the solar cell than for non-concentrated radiation. Also the concentrated radiation can be processed with greater efficiency. Special solar cells called concentrator cells make use of this phenomenon and because of the higher temperatures semiconductors with larger bandgap are advantageous in this case, such as GaAs.[1.16]

Chapter 2: Experimental Methods

This chapter briefly describes the various equipment and processes that were used during the course of this thesis. GaAs p-n junction nanowires were grown on an n-type GaAs substrate using molecular beam epitaxy (MBE) by the vapour-liquid-solid (VLS) method. These wires were characterized using scanning electron microscopy (SEM), acquiring details of their surface density, height, diameter, etc. This was followed by spinning a polymer onto the nanowire sample that completely covered the wires. SEM was again used to image a cross-section of the polymer-covered sample and the height of the polymer above the top of the nanowires was obtained. The polymer was then etched back by reactive ion etching (RIE) using oxygen plasma to expose the top of the wires for making electrical contacts. Au or indium tin oxide (ITO) was used for the top contact while Ni/Ge/Au (250 Å, 500 Å and 1200 Å, respectively) was used for the bottom contact, deposited by an electron beam evaporation system. Current-voltage (I-V) curves were then obtained through this arrangement of the basic solar cell, with and without illumination, using the Solar Simulator from Newport Oriel Instruments, Model 69907. This device uses a 150 W ozone-free xenon lamp, and produces a 1.3 inch (33 mm) diameter collimated beam. [2.1]

2.1 Molecular Beam Epitaxy (MBE)

Nanowires in this thesis were grown by molecular beam epitaxy (MBE). MBE was developed in the early 1970s as a means of growing high-purity, thin epitaxial layers

of compound semiconductors.[2.2, 2.3] Since then it has evolved as a very popular and advanced technique for growing III-V compound semiconductors as well as several other materials including metals and insulators. MBE can produce high-quality layers with very abrupt interfaces and good control of thickness, doping, and composition, making it a valuable tool in the development and fabrication of sophisticated electronic and optoelectronic devices.[2.4]

In MBE thin film crystallization occurs via reactions between thermal energy molecular or atomic beams of the constituent elements and a substrate surface which is maintained at an elevated temperature.[2.5] In order to obtain high purity layers it is critical that the material sources be extremely pure and that the entire process be done in an ultra-high vacuum environment.

The composition of the grown epilayer and its doping level depend on the relative arrival rates of the constituent elements and dopants, which in turn depend on the evaporation rates of the appropriate sources.[2.5] The slow growth rate of about 1 monolayer per second ensures the surface migration of the impinging species on the growing surface, and results in a very smooth film. The composition and doping of the growing structure can be controlled by changing the flux of the incoming beam just by opening and closing mechanical shutters in front of the beam with the operation time of approximately 0.1s which is much shorter than the growth time of one monolayer.[2.6] The intensity of the flux of every component or dopant is managed by carefully varying the temperatures of the cells via PID controllers. PID Temperature Controllers monitor the MBE effusion cell temperature and regulate the power supply output. They allow the

three parameters-Proportional band, Integral time constant and Derivative time constant (PID) to be tuned to the specific heater filaments and temperature range used. This enables the cells to achieve excellent flux stability.[2.7]

The basic schematic of an MBE system is shown in Figure 2.1 below. The epitaxial growth occurs by the interaction of one or several molecular or atomic beams on a substrate of heated crystalline material. The solid source materials are placed in evaporation cells to provide an angular distribution of atoms or molecules in a beam. The substrate is heated to the necessary temperature and, when needed, continuously rotated to improve the growth homogeneity. If the total pressure does not exceed 10^{-5} Torr, the molecular beam condition that the mean free path of the particles should be larger than the geometrical size of the chamber is fulfilled easily.

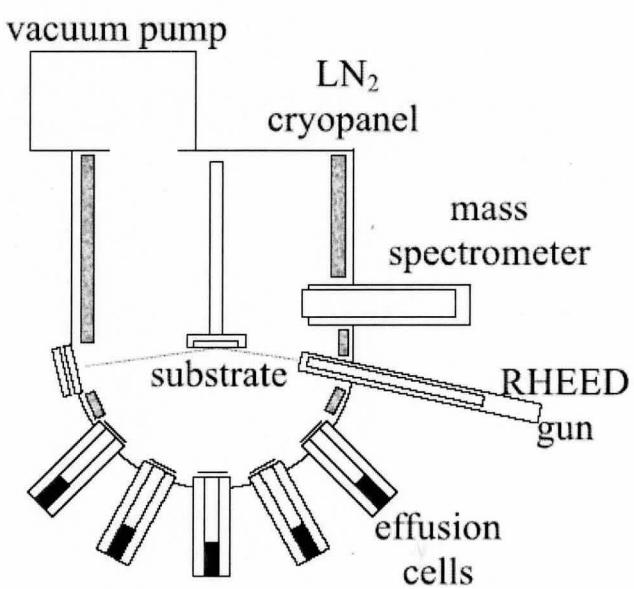

Figure 2.1. Basic schematic of a typical MBE system.[2.6]

2.2 Vapour-liquid-solid (VLS) Method For Fabrication of Nanowires

In its basic form, the vapor-liquid-solid (VLS) growth process comprises a metal seed particle acting as a catalyst for the epitaxial growth of semiconductor material on a suitable substrate.[2.8] In the VLS process, originally proposed by Wagner and coworkers, crystals of a unique form called "whiskers" or "filamentary crystals" result from anisotropic growth from the vapor. Such crystals have a lengthwise dimension that is orders of magnitude larger than that of the cross-section.[2.9] The reaction of iodine and silicon in a closed quartz tube gave rise to whiskers as small as 500 Å and as large as 100 μm or more.[2.10]

In the VLS process nanowires are grown in two steps. First, the seed particle forms a liquid solution with the crystalline material to be grown from the vapor. This solution becomes a preferred deposition site for the vapor which causes the liquid to become supersaturated. The second step is the occurrence of crystal growth by precipitation from the supersaturated liquid at the liquid-solid interface. This VLS mechanism produces unidirectional crystal growth perpendicular to the solid-liquid interface. The presence of the seed particle is very critical for VLS growth. The requirements for the particle include:

1) Must form a liquid solution with the crystalline material at the deposition temperature.
2) It should be inert to the chemical reaction products.

3) The wetting characteristics arising from the interfacial energies (vapor-solid, vapor-liquid, and liquid-solid) strongly influence the shape of the growing crystal. Large area growth needs small contact angle while whiskers need large contact angle.
4) In VLS growth of compound crystals, the seed can be one of the components of the compound itself.

For VLS growth of group III-V semiconductors, gold is frequently used since it forms a eutectic with these, and also its solubility in III-V compounds is negligible. Heating the sample above the eutectic melting point of the metal/semiconductor, results in melting and coalescing of the metal catalyst to form beads on the substrate surface.

During deposition the molten metal catalyst becomes the preferred site for incorporation of vapor. When vapor is fed into the molten catalyst droplet it becomes supersaturated with the growth species. Precipitation occurs at the liquid-solid interface and one-dimensional growth of wires or whiskers is initiated under the melt. In VLS, nucleation is confined under the catalyst. In metal catalysts with nanometer dimensions most of the time nucleation sites are so limited that there is only one wire under the melt, but occasionally multiple sites have also been observed and hundreds or thousands of wires have been observed from micron sized drops.[2.11, 2.12]

With appropriate metal, negligible incorporation into the wire can be achieved such that the metal rides on top of the wire during growth. The location and diameter of the wires are defined by the size and placement of the metal catalyst while the length of the wire is determined by the growth time. Because the growth is concentrated under the

metal catalyst, high aspect ratio wires are possible. Both nanowires (diameters as small as 3 nm) and microwires (diameters larger than 100 nm) have been produced with wire lengths in excess of several microns.[2.13]

Growth of wires may be sustained by adatoms supplied via three pathways as shown in Figure 2.2. [2.13] (a) and (b) result from the direct impingement of the growth species on the catalyst. In (a), the species diffuse on the surface of the Au particle in a random walk manner until they either desorb or encounter the growth interface. At this point the adatoms may incorporate into the wire crystal through diffusion along the crystal-wire interface. The path (b) consists of bulk diffusion through the gold particle. The third path (c) consists of growth species impinging on the substrate surface which may diffuse in a random walk manner to the base of wires and then along the wire sidewalls up to the growth interface. Once again the adatoms will either incorporate in the crystal by diffusing along the crystal then along the catalyst-wire interface or continue their walk on the surface to eventually desorb or diffuse in the Au particle. [2.13]

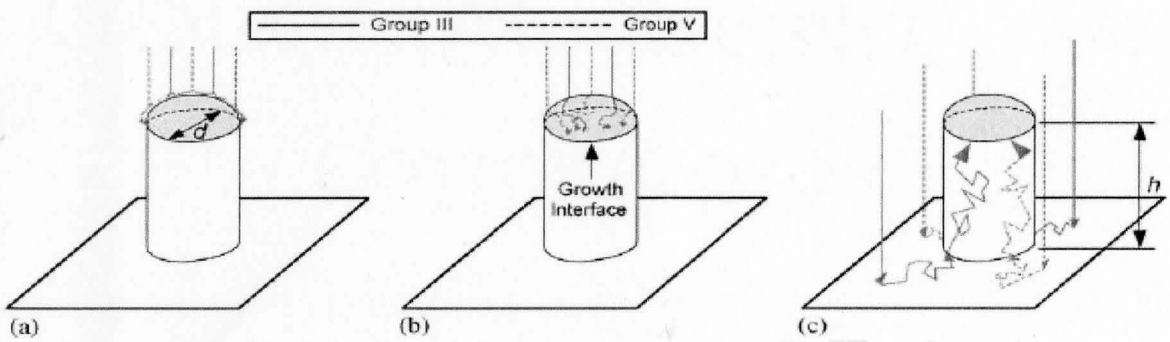

Figure 2.2. Mass transport mechanism of growth species to the Au-wire interface.[2.13]

2.3 Scanning Electron Microscopy (SEM)

SEM was used to produce high magnification images of the nanowires and nanowire-based devices in this thesis. SEM produces a highly magnified image by using electrons instead of light to form the image. It has many advantages over the traditional microscopes including large depth of field allowing more of the specimen to be in focus at one time, higher resolution so that closely spaced specimens can be magnified at much higher levels and more control to the user over degree of magnification because of the use of electromagnets rather than lenses. [2.14]

A beam of highly energetic (0.1-50 keV) electrons impinges on a sample surface resulting in several interactions including elastic scattering from the specimen with no loss of energy, absorption by the specimen giving rise to secondary electrons of very low energy together with X- rays, and absorption giving rise to the emission of visible light (an effect known as cathodoluminescence). Incident electrons may also give rise to electric currents within the specimen. All these effects can be used to produce an image. By far the most common, however, is image formation by means of the low-energy secondary electrons.[2.15] Since the bombarding electron beam is scanned in the x-y plane, an image for each of these different processes can be mapped with a suitable detector.

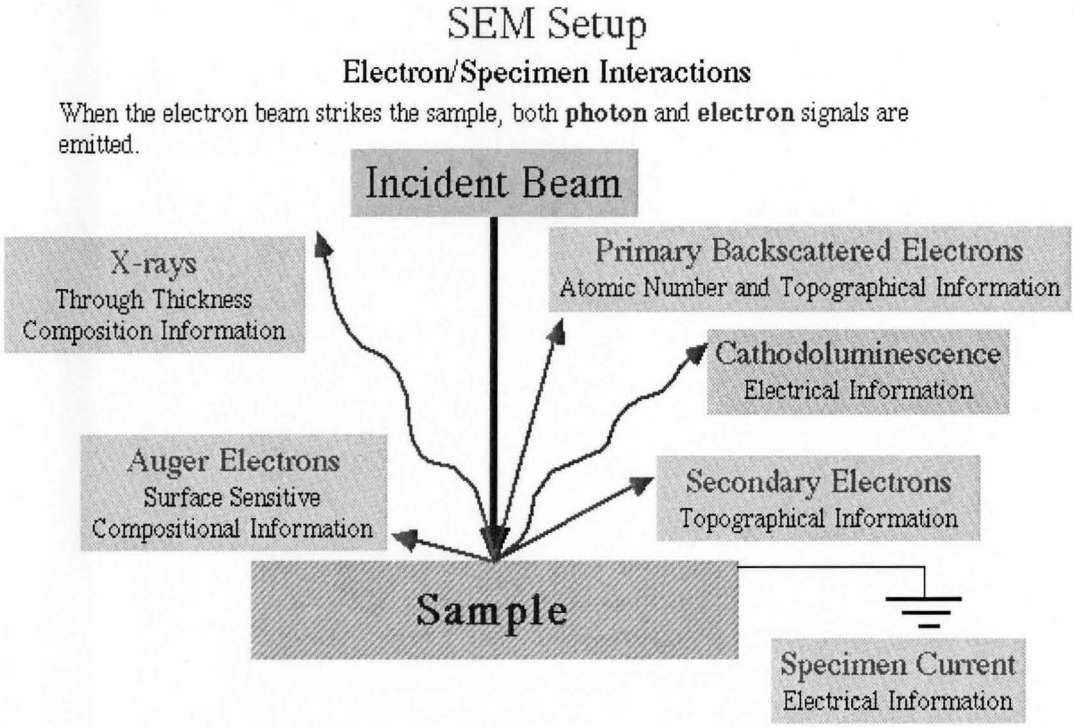

Figure 2.3. Incident electron beam and specimen interactions. [2.16]

The detector for secondary electrons that is standard to all basic SEM records the topography of the surface under observation with resolution on the order of 1-2 nm and magnification range from 10x to 500,000x. In addition to this, appropriate detectors can give information on phase, composition, electrical, optical, thermal and other properties of the specimen with excellent resolution.

In SEM, vacuum is required in the column to eliminate instability in the beam, hindrance in the transmission of the beam and to reduce the formation of compounds condensing on the sample surface caused by the presence of the gases.[2.14]

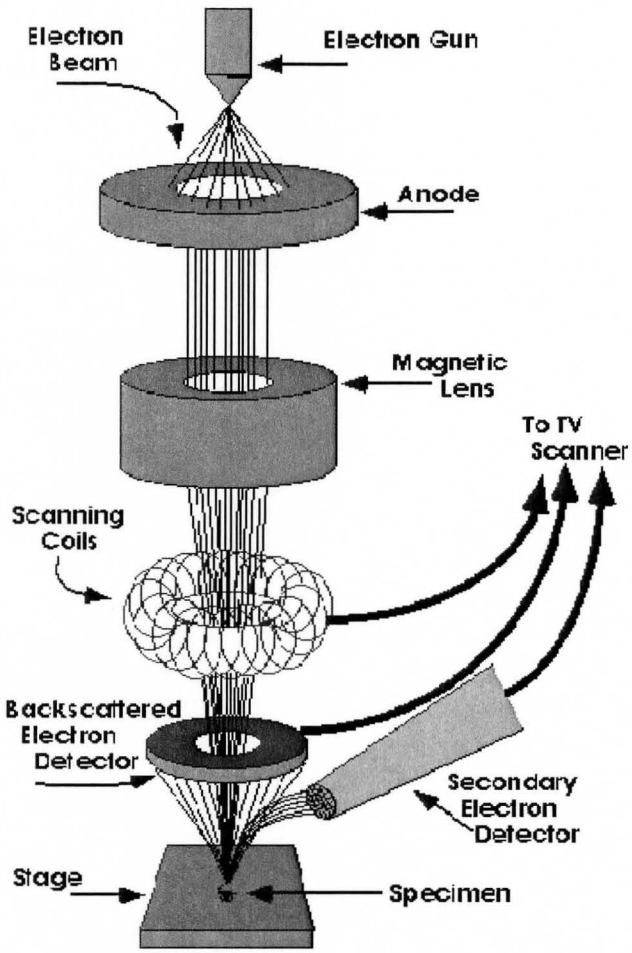

Figure 2.4. Schematic diagram showing SEM operation. [2.14]

The incident beam in SEM is scanned over the specimen in a series of lines and frames called a raster, just like the (much weaker) electron beam in an ordinary television. The raster movement is accomplished by means of small coils of wire carrying the controlling current (the scan coils).

The secondary electrons are selectively attracted to a grid held at a low (50 volt) positive potential with respect to the specimen. A disc is held behind the grid at about 10 kilovolts positive with respect to the specimen. The disc consists of a layer of scintillant

coated with a thin layer of aluminum. Emission of light occurs from the scintillant when secondary electrons pass through the grid and strike the disc. From here the light is led down a light pipe to a photomultiplier tube which converts the photons of light into a voltage. The strength of this voltage depends on the number of secondary electrons that are striking the disc. Thus a voltage signal of a particular strength is formed by the secondary electrons produced from a small area of the specimen. The voltage is led out of the microscope column to an electronic console, where it is processed and amplified to generate a point of brightness on a cathode ray tube (CRT) screen. An image is built up simply by scanning the electron beam across the specimen in exact synchrony with the scan of the electron beam in the CRT. [2.17]

The SEM does not contain objective, intermediate and projector lenses to magnify the image as in the optical microscope. Instead magnification results from the ratio of the area scanned on the specimen to the area of the CRT screen. Increasing the magnification in an SEM is therefore achieved quite simply by scanning the electron beam over a smaller area of the specimen. [2.18]

An SEM can be fitted with X-ray analysis equipment. Computer analysis of a characteristic wavelength or energy spectra emitted from the specimen when it is bombarded with electrons makes it possible to accurately measure the nature and quantity of different elements in the material. This technique is of great importance in material science because of the fact that an area as small as 1 μm^2 can be analyzed with precision. Some SEM systems can also take advantage of back scattered electrons generated by the probe beam to perform material composition analysis.

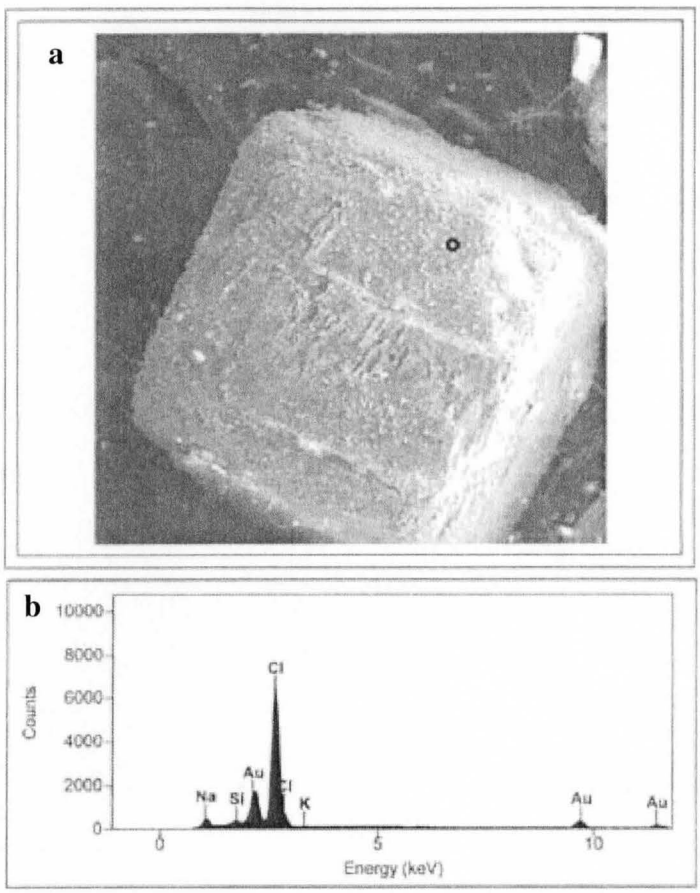

Figure 2.5. (a) Scanning electron microscope image of salt crystals. (b) Spectrum of the energy of characteristic X-rays emitted from the salt (NaCl) crystals. In the energy spectrum the X-ray peaks from sodium (Na) and chlorine (Cl) are identified. [2.18]

2.4 Reactive Ion Etching (RIE)

Reactive ion etching (RIE) is a plasma-based process developed to physically imprint semiconductor circuit features into the surface of a wafer. RIE was used in this thesis to remove photoresist polymer during nanowire device processing. The ionization of a controlled mixture of gases localized above a sample serves to remove any exposed portion of the sample's surface area via a combination of chemical reaction and physical

bombardment.[2.19] RIE can be well suited to the fabrication of features with extremely deep, vertical side walls, and highly consistent critical dimensions. RIE is one of the various fabrication techniques that make use of the formation and properties of plasma, sometimes called "glow discharge". The plasma-based processes are not thermal and the dynamics of film formation or etching cannot be described by equilibrium thermodynamics. The plasmas for these processes are typically formed by partially ionizing a gas below atmospheric pressure. They are mostly weakly ionized with an ionization factor of 10^{-5} to 10^{-1}. For deep reactive ion etching however the ionization fraction approaches 0.3 to 1 at high powers. Electrons are the dominant charge carriers in plasmas because they can respond to electric fields more readily because of their low mass. For many calculations with these plasmas it is typical to deal only with electrons assuming ions to be virtually immobile.[2.17]

In RIE, a reactive gas species such as CF_4 or SF_4 is added to the chamber, and when plasma is formed by the applied rf potentials, the gas molecules are broken down into a number of fragments and radicals. These ions are accelerated towards and react at the surface of the material being etched forming another gaseous material. This is called the chemical part of the reactive ion etching. Another part of reactive ion etching is the physical part that is similar to a sputtering deposition process. If the ions have high enough energy, they can knock atoms out of the material to be etched without a chemical reaction. Developing a dry etching process that can balance the chemical and physical etching is very complex since many parameters need to be adjusted. Samples in most RIE systems are placed on the powered electrode and exposed to the flux of ions from the

plasma as well as the more isotropic flux of gas species that may also be formed within the chamber.

During the process of RIE gaseous species from the plasma react with the surface atoms forming compounds or molecules, and leave the surface if the vapor pressure is high enough or as a result of ion bombardment. This reaction may be rate-limited by the production rate of reactive species in the plasma, by the surface reaction rate or by emission rate of products to be etched. For maintaining the anisotropy and directionality of the etching process, ion bombardment has been found to be very useful as it may clean the surface, allowing the reaction to occur or stimulate the reaction itself or help in desorbing or detrapping the product molecules. F-based plasmas are normally used for isotropic etching while Cl and Br-based plasmas are used for anisotropic etch profiles.

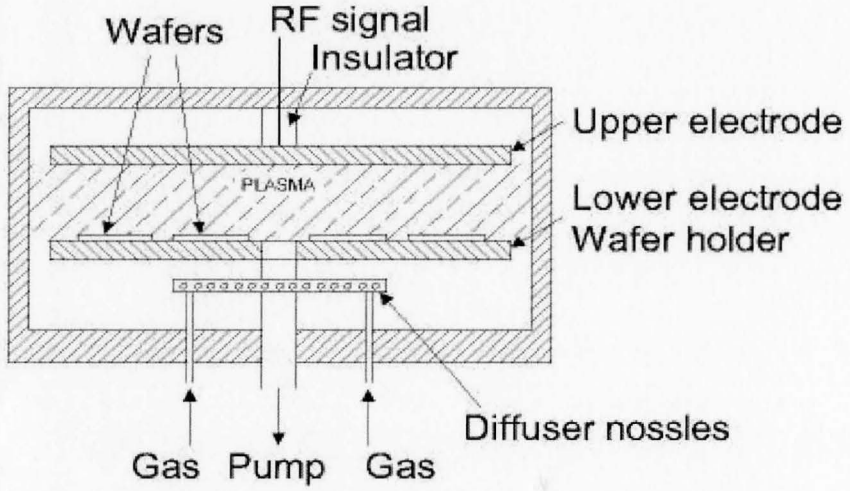

Figure 2.6. Typical parallel plate reactive ion etching system. [2.20]

The quality of features etched by RIE depends on a number of process parameters, including gas flow rates, chamber pressure, RF power, chamber temperature, and pattern density. For the current project, the "Technics Micro RIE series 800" system was used to etch away the SU8 2 resist from the tops of the nanowires for contacting purposes, at the rate of 1000 Å per minute. The parameters used were:

Oxygen gas flow rate (sccm):	28
RF Power (W):	100
Chamber pressure (mTorr):	352
Time (min):	1
Base Press (mTorr):	42

2.5 Sputter Coating System

Sputtering was used in this thesis to deposit indium tin oxide (ITO) as a transparent conducting oxide for the top electrode of the nanowire solar cells. Sputtering is the erosion process of a target material that normally resides as a cathode, and occurs in an environment of gaseous glow discharge between the anode and the cathode when it is bombarded with fast heavy particles. This results in the omni-directional deposition of the sputtered atoms forming coatings of the original cathode material on the surface of the sample and work chamber. In this process the momentum of the bombarding ions is more important than their energy. Sputtered atoms travel until they strike a substrate, where they deposit to form the desired layer. As individual atoms they are chemically active and readily form compounds with the ions and atoms of the bombarding gas. For this reason inert argon is used as the bombarding gas. In some applications however, a reactive gas is

purposely added to argon so that the deposited film is a chemical compound, and not the elemental target materials.[2.21]

The basic idea of sputtering involves the use of plasma to introduce a source material into a vapor state. The plasma consists of a high density of gaseous ions. When the plasma strikes the surface of the source material, it has enough energy to erode particles of the source material into a vapor or gaseous phase. The vapor phase of the source material can then be deposited onto a substrate within the system.

Sputtering is a proven, successful method of coating a variety of substrates with thin films of electrically conductive or non-conductive materials. One of the most striking characteristics of sputtering is its universality. Since the coating material is passed into the vapor phase by a physical rather than a chemical or thermal process, virtually any material can be deposited. Direct current is used to sputter conductive materials, while radio frequency is used for non-conductive materials.[2.21] This process is enhanced in sputter coaters for use in scanning electron microscopy where one objective is to provide an electrically conductive thin film over the specimen to be viewed. Such films inhibit "charging", reduce thermal damage, and enhance secondary electron emission.[2.22] For such specimens to be used in SEM, the most commonly used arrangement in a DC sputter coater is to make the negative cathode the target material to be sputtered (typically gold), and to locate the specimens to be coated on the anode (which is usually grounded to the system). The desired operating pressure is obtained by a pump, usually a two stage rotary vacuum pump, with an inert gas, such as argon admitted to the chamber by a fine control (leak) valve.

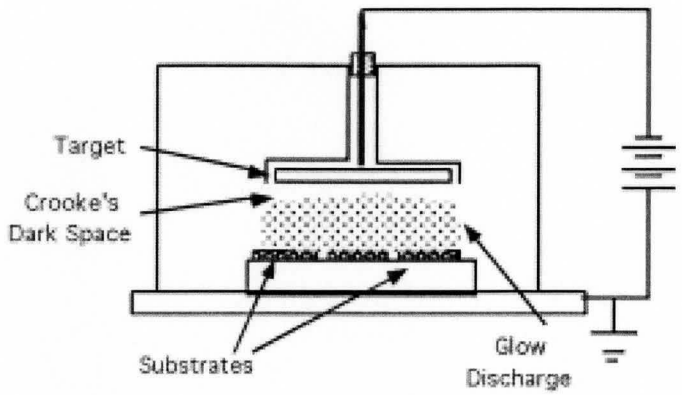

Figure 2.7. Schematic diagram of a sputtering system. [2.23]

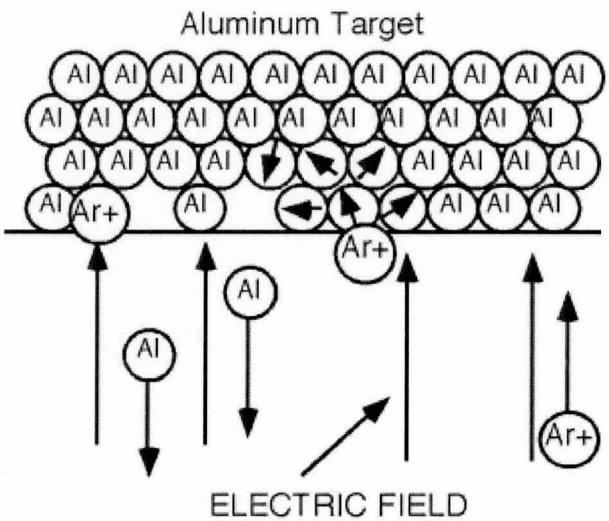

Figure 2.8. Sputtering mechanism showing erosion of Al atoms for deposition. [2.24]

Sputtering was also used for making top contacts of indium tin oxide (ITO) on the nanowire samples to be used as solar cells. For this purpose the "2" inch MAK source

sputtering gun from US Inc." was used. The sputtering thickness was ~120-240 nm. The normal sputtering condition was 20 Watts of power and 1.0 mTorr working pressure with Ar gas, without substrate heating.

2.6 Electron Beam Evaporation

Electron beam evaporation is the most versatile means of thin film deposition, with numerous advantages over other competing techniques such as precise control of low or high deposition rates, excellent material utilization, co-deposition and sequential deposition systems and a uniform low temperature deposition. The electron beam used in this technique offers higher evaporation rates, freedom from contamination, precise rate of control at very low deposition levels, precise film composition, and cooler substrate temperatures.[2.25]

In this technique the source or material to be deposited is heated by bombarding a very high energy electron beam that heats and then evaporates a very pure source, which is then allowed to condense on the substrate. The beam is generated by an electron gun which uses the thermionic emission of electrons produced by an incandescent filament (cathode). A high potential difference of several kilovolts accelerates the emitted electrons towards an anode, which could either be the crucible containing the source or a near perforated disc. A magnetic field helps position the electrons directly on the source. It is possible to obtain a very localized heating on the source with a high density of evaporation power (several kW). This allows control of the evaporation rate from very low to very high values as well as a chance to deposit materials with high melting point.

Contamination problems from degassing and heating are avoided by cooling the crucible. [2.26]

The entire process takes place inside of a vacuum chamber for the evaporation and condensation processes to occur with minimum or no contamination.

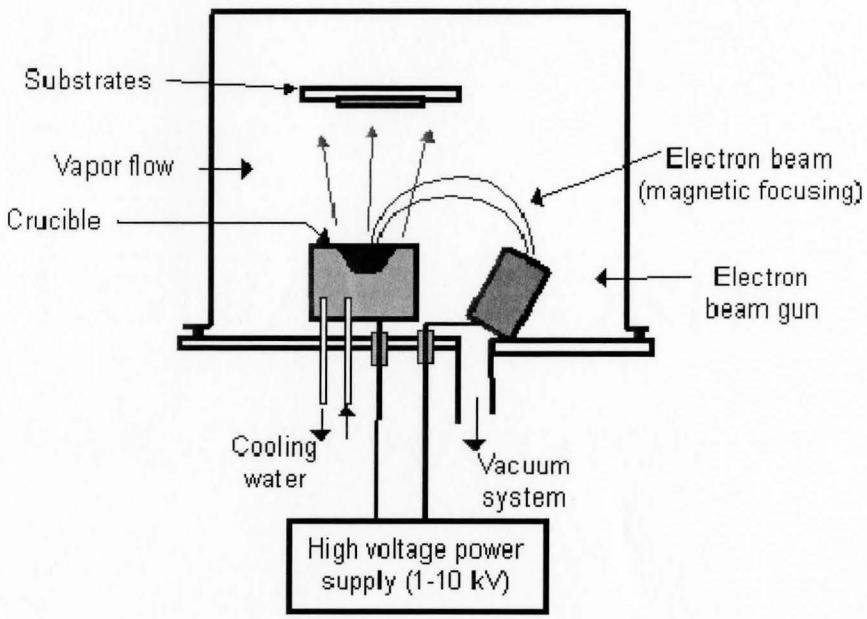

Figure 2.9. Schematic diagram of an Electron Beam Evaporator. [2.26]

The e-beam evaporator system used for the purpose of metallizing the bottom of the n-type GaAs wafer was the system by "UHV Instruments, ID 2500 Ion Beam Drive, Commonwealth Scientific Corporation". Pt, Cr, Au, Ni , and Ge can be deposited by this evaporator. As part of the current research 250 Å Ni, 500 Å Ge and 1500 Å Au were deposited on the bottom side of the sample as the standard n-type contact.

Chapter 3: Nanowire Solar Cells

This chapter describes the fabrication of nanowire-based solar cells.

3.1 Nanowires

Nanowires (NWs) were grown by MBE using the VLS method as described in Sections 2.1 and 2.2. The NWs were grown on a 3" n-type GaAs substrate (n~10^{18} cm^{-3}, supplied by AXT). The NWs were grown at a substrate temperature of 550 °C and V/III flux ratio of 1.5. The growth duration was 30 minutes, consisting of 20 minutes with n-type doping and 10 minutes with p-type doping. Nominal doping levels were 10^{18} cm^{-3} achieved using elemental Si and Be from solid source effusion cells for n-type and p-type doping, respectively. Under these conditions, the NWs have both axial and radial growth resulting in the core-shell structure illustrated in Figure 3.1. This is evident from the tapered morphology of the NWs illustrated by the SEM images in Figure 3.2. The average NW diameter was 100nm and height was between 2 to 2.5 μm. The as-grown NW sample appeared black in color implying excellent optical antireflection property of the wires which is one basic requirement of solar cells.

In addition to the NW growth, some 2-D film growth also takes place simultaneously between the NWs as shown in Figure 3.1.

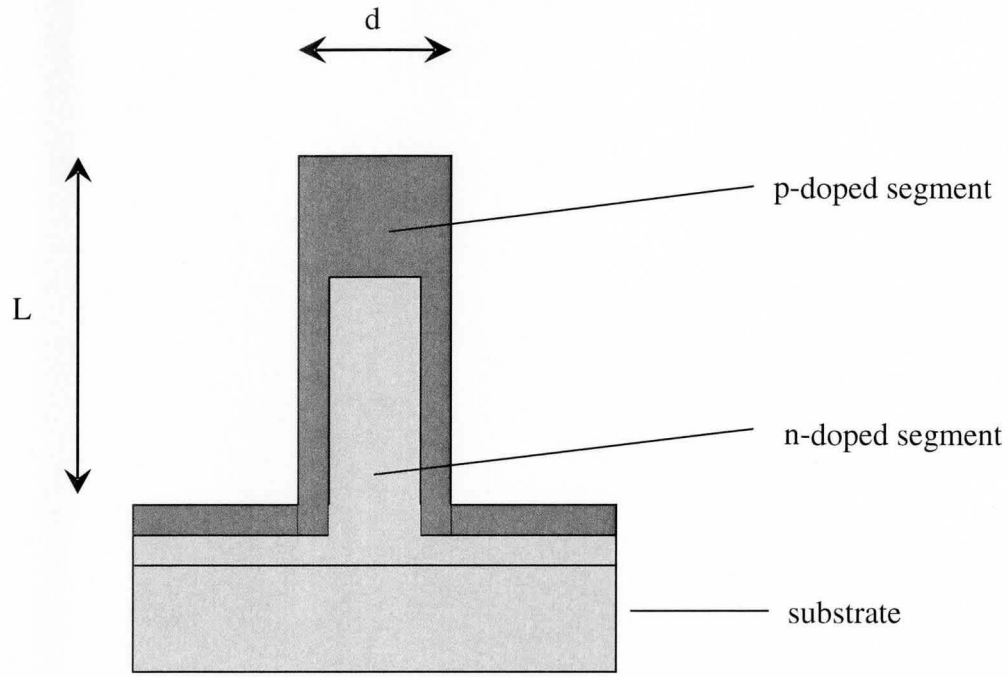

Figure 3.1. Illustration of core-shell p-n junction NW of height L and diameter d.

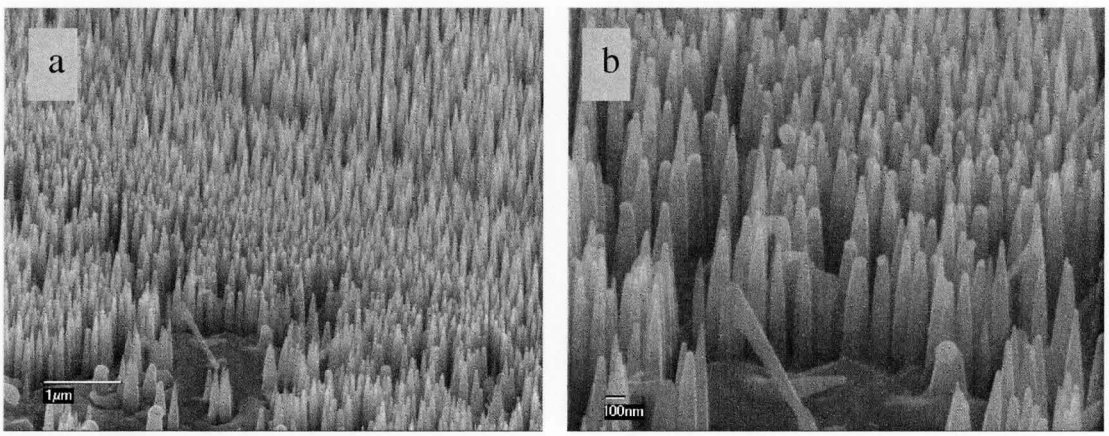

Figure 3.2. 45° tilted view of GaAs p-n junction NWs grown on a (111) B GaAs substrate by VLS method using MBE.

3.2 Solar Cell Device Processing

The step-by-step approach towards the fabrication of solar cells is shown in the following steps: [3.1]

Step 1: Growth of p-n junction NWs on (111) B GaAs substrate by VLS method using MBE.

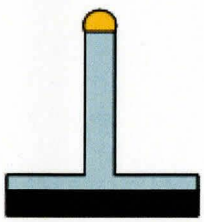

Step 2: Metallize for bottom contacts.

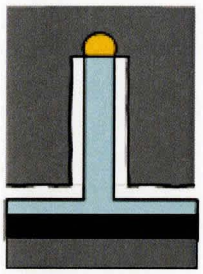

Step 3: Deposition of polymer onto the nanowires.

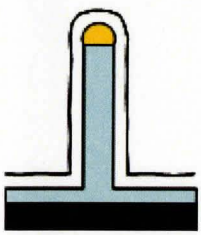

Step 4: Reactive ion etching (RIE) to remove the polymer and expose the NW tops for metal contacts.

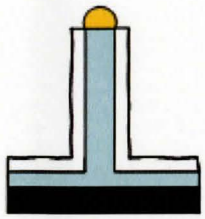

Step 5: Metallize for top contacts.

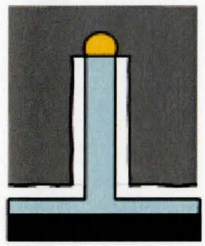

Following the above mentioned steps, the NWs were processed into the solar cell device shown in Figure 3.3 and described below.

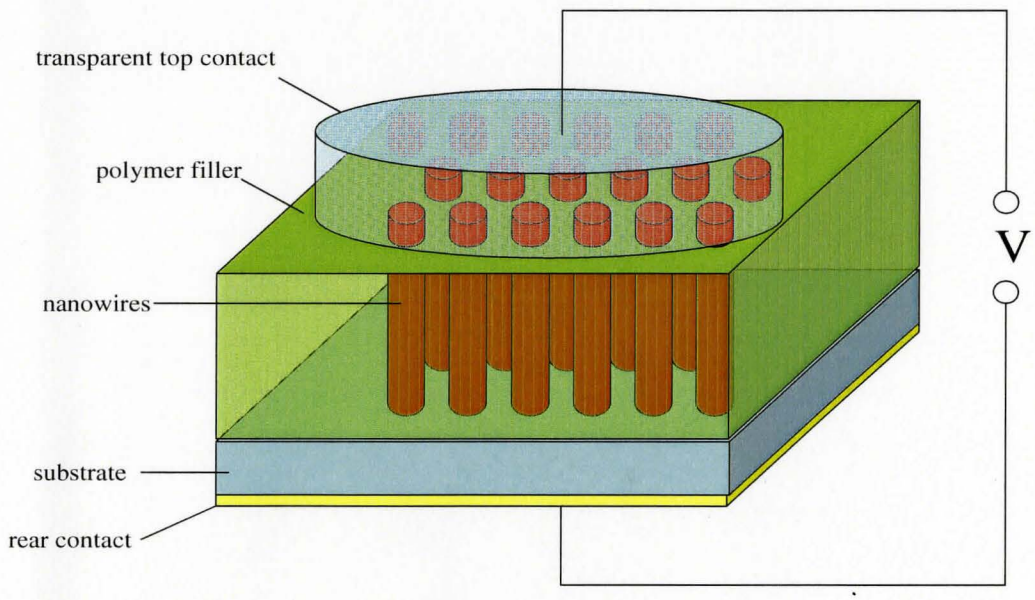

Figure 3.3. Conceptual illustration of a nanowire solar cell.

After growing core-shell p-n junction NWs by the VLS method using gas source MBE as explained earlier in chapter 2 (step 1), a standard n-type electrical contact was formed on the bottom of the substrate (step 2) by electron beam evaporation system "UHV Instruments, ID 2500 Ion Beam Drive, Commonwealth Scientific Corporation" with the thickness of the three layers Ni, Ge, and Au being 250 Å, 500 Å and 1500 Å respectively. After deposition, the contact was annealed with Si wafer as capping at 380 °C for 30s using an AG Associates Mini-Pulse rapid thermal annealing (RTA) furnace under an atmosphere of nitrogen.

After formation of the bottom electrode, the NWs were embedded in a polymer (step 3) to fill the voids between NWs. The polymer acted as a mechanical support for the top contact as described below. The desired properties of the polymer include transparency to visible light for minimal light loss by absorbance, ability to spin-coat a uniform layer of approximately 2 μm thickness, and capability of removal by reactive ion etching with oxygen plasma (described later). The polymers S1818, PDMS, PMMA, and SU8 2 as summarized in Table 3.1 were used as potential candidates for this purpose. Also S1818, pf 5070, EGC 1700 and S1827 were used later for NW transfer onto a flexible substrate.

Table 3.1 Polymer candidates investigated for NW embedment and NW transfer onto a flexible substrate.

Polymer	Supplier
S1808	Shipley Inc.
S1818	Shipley Inc.
S1827	Shipley Inc.
PDMS	PDMS
Pf 5070	3M
PMMA	3M
SU8 2	MicroChem
EGC 1700	3M

Characterization of the samples after spin-coating the different polymers was done with JEOL JSM-7000F field emission scanning electron microscope (FE-SEM) in the secondary electron mode. Figure 3.4 shows the SEM images of the NW samples with PDMS, S1808, and PMMA.

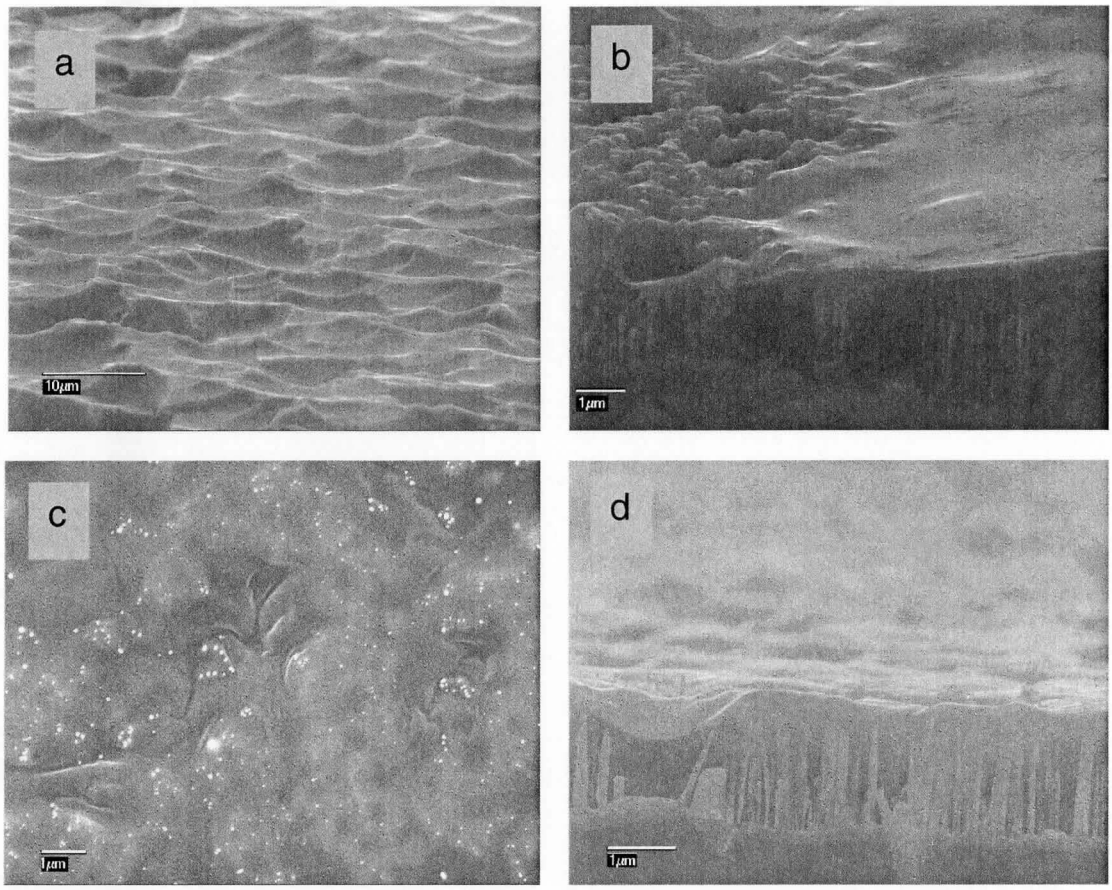

Figure 3.4. SEM images of NW sample with different spin-coated polymers. (a) NW sample with PDMS spin-coated at 7500 rpm for 90 s. (b) S1808 on NW sample at 5500 rpm, for 50 s. (c) Top view of PMMA spin-coated at 3000 rpm for 30 s on NW sample. (d) Side view image of PMMA on NW sample.

The above images show that none of the three polymers, PDMS, S1808 and PMMA served our purpose. PDMS could not be spin-coated to give a thin enough layer, and different trials with different speeds and time repeatedly resulted in very thick, non-uniform layer. S1808 resulted in a non-uniform layer with repeated trials as shown in Figure 3.4(b). PMMA could be spun to give a thin but non-uniform layer so that the top of the wires could be exposed, but a tilted view showed that the polymer sat on top of the wires and failed to fill out the space between them.

However, repeated experiments established SU8 2 as the most suitable polymer fulfilling the above stated requirements for our conceptual solar cell. Figure 3.5 provides the spin-coat thickness versus spin speed for the SU-8 family of polymers. When spun at a speed of 4500 rpm for 60 s, SU8 2 gave a fairly uniformly coated layer of height close to 2.5 μm, showing some of the taller wires exposed. This was done by placing a NW sample on the spinner and SU8 2 poured onto it using a pipette. The SU8 2 was left on the sample for 5 minutes and then the spinner was turned on at a speed of 4500 rpm for 60 s. A uniform layer of the polymer was coated, filling the space between the NWs as desired, as shown in the characterization of the sample by SEM in Figure 3.6.

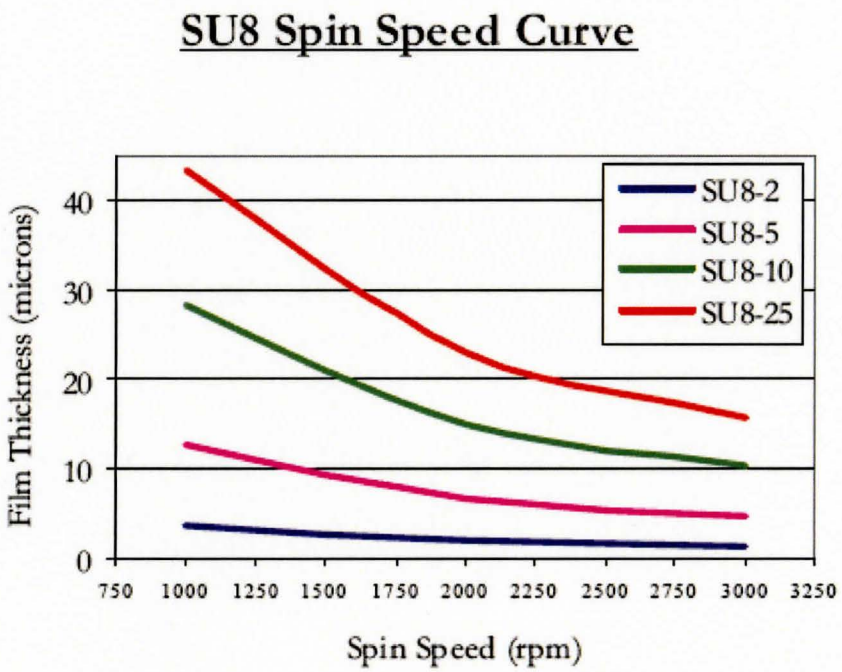

Figure 3.5. Thickness versus spin speed for SU-8 resists.[3.2]

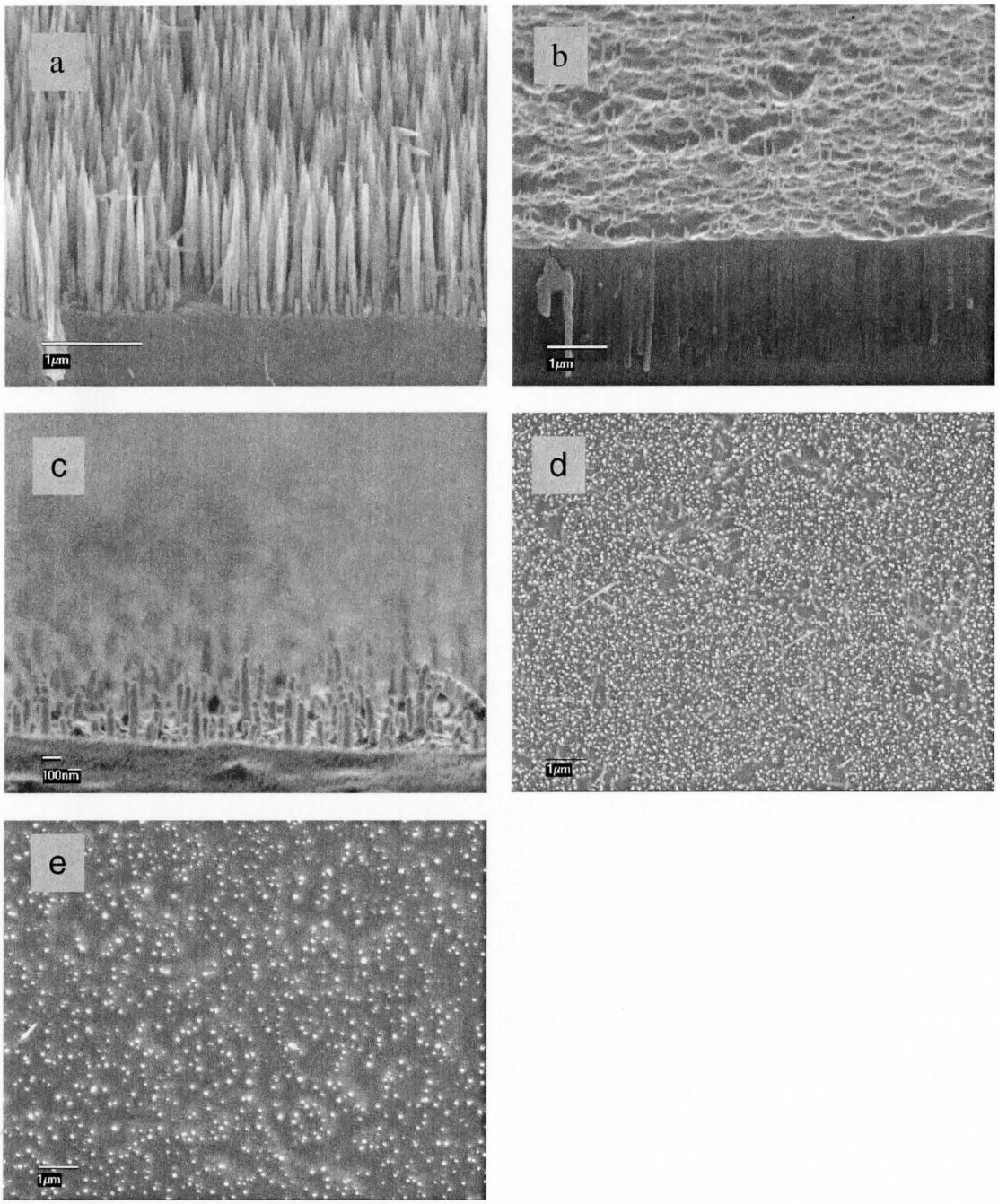

Figure 3.6. SEM images showing NW sample before and after spin-coating with SU8 2. (a) Tilted view of as-grown NW sample. (b) Tilted view of NW sample after SU8 2 spin-coating. (c) High magnification tilted view of top of NW sample with SU8 2. (d) Top view of as grown NW sample. (e) Top view of NW sample after spin-coating SU8 2.

The above images show a comparison between the as-grown samples and those having SU8 2 spun at 4500 rpm for 60 s, clearly indicating the success of SU8 2 over other polymers used for the same purpose. The images also show that a considerable density of NWs is exposed for contacting, which will be improved by the RIE etching process carried out later to expose more wires as well as to eliminate any polymer coating on the top of wires.

As mentioned above, the next step involved removing the polymer from the top of the NWs by reactive ion etching using the "Technics Micro RIE Series 800" oxygen plasma system. This step allowed the top of the NWs to be exposed for the top electrode deposition. The rate of polymer etching was found to be 1000 Å per minute. To achieve this, SU8 2 was spun onto a Si substrate using the same conditions as on the NW sample, and the thickness of the layer was measured by SEM and an "alpha stepper" thickness profilometer. This was followed by etching the polymer using the oxygen plasma system mentioned above for 30 seconds and the polymer thickness again measured by SEM and alpha stepper. Again the polymer was etched for 1 minute keeping the etch conditions constant (mentioned below) and its thickness measured. Repeating the same trial for 2 mins of etching proved that SU8 2 could be etched at a rate of 1000 Å per minute, using an oxygen gas flow rate of 28 sccm, vacuum chamber pressure of 352 mTorr, with base pressure being 42 mTorr for 1 min and the RF power equal to 100 Watts. Figure 3.6 shows the NW sample after going through the identical etching process. When the results in Figure 3.7 are compared to that in Figure 3.5, etching by SU8 2 can be seen to be successful as it exposes a considerable number of wires for top contacting.

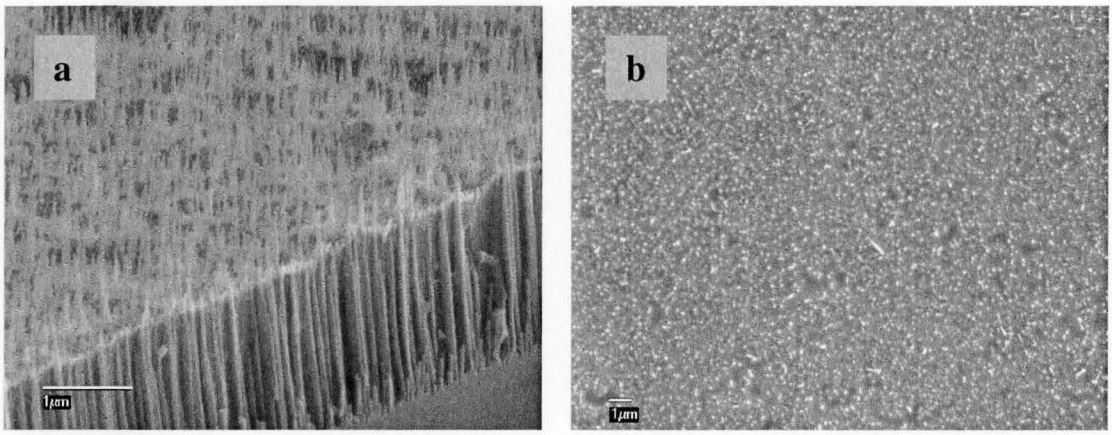

Figure 3.7. SEM images of NW sample with SU8 2 spin-coated followed by etching back at the rate of 1000 Å per minute for 1 minute. (a) Tilted cross-sectional view of the NW sample showing etched NW tops. (b) Top view of the sample after being etched.

Finally, after the polymer etching by RIE, an electrode was formed at the top of the NWs by sputter deposition for electrical characterization. Various top electrode materials were deposited in the form of dots through a shadow mask. Two different shadow masks were used for this purpose: first one with holes having a diameter of ~200 μm separated by 800 μm while another one with holes of diameter around 800 μm and 200 μm apart. Experiments for I-V curves with the first type of mask did not give any considerable results since the probe size of the I-V measurement apparatus used was found to be comparable to the dot size, and ended up in damaging the whole area of the dot and hence the NWs under it. The second type of mask with more than four times the area available for contact gave better results.

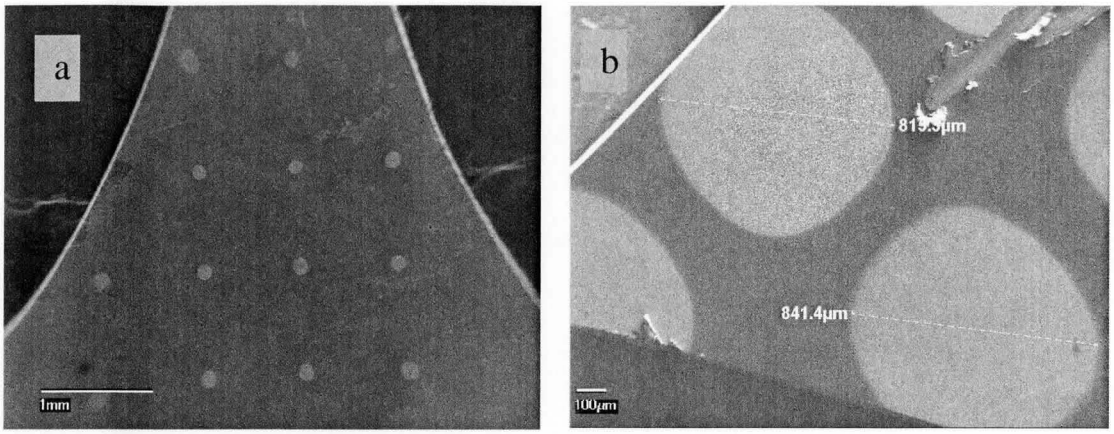

Figure 3.8. Top view SEM images showing NW samples with Au dots using the two different shadow masks. (a) SEM image of NW sample with Au dots deposited by e-beam evaporation using shadow mask with holes around 800 µm apart and 200 µm in diameter. (b) SEM image of NW sample with Au dots using shadow mask with holes around 800 µm in diameter and 200 µm apart.

Three types of top contacts were investigated: (1) a standard p-type contact consisting of 25 nm Ti, 50 nm Pt, and 150 nm Au deposited by electron beam evaporation since the NWs were p-n junctions with the top of the wires with p-type doping; (2) 700 nm Au deposited by electron beam evaporation; and (3) 400 nm indium tin oxide (ITO) deposited by sputtering. The sputtering system and electron beam evaporation system used in the process are described in Sections 2.5 and 2.6 respectively. For the devices described in this thesis, none of the top contacts were annealed since the SU8 2, according to the manufacturer's specifications, could not withstand anneal temperatures above 200 °C appropriate for alloying metal contacts. For example, at 300-315 °C, the SU-8 would experience 5% weight loss.[3.3]

3.3 I-V Measurements

The current-voltage (I-V) curve measurements were done by "Keithley Model 2400 LV SourceMeter" which has precision voltage and current sourcing as well as measurement capabilities. It is both a highly stable DC power source and a true digital multimeter. The whole setup used for taking these measurements along with the probe is shown in Figure 3.9 below. The prepared sample was placed with the NWs facing upwards on a copper plate attached to a movable stage to help adjust the position of the sample according to the light source that illuminated the sample. A probe made of tungsten tip with a nickel shank, tip size $\approx$ 0.005" attached to one terminal of the voltage source through a tip manipulator was made to contact the plate firmly. For the top contact a second probe of same dimensions attached to the second terminal of the voltage source was placed in contact with the contact pad, the ITO dot in this case. Voltages between -10V and +10V were applied to the sample through the probes and the resulting current was measured and plotted against the applied voltage, resulting in current-voltage (I-V) graphs. The system was equipped with Labview software to measure the I-V curves. These curves, shown in Figure 3.9, were measured under dark and AM 1.5 illumination conditions using a Newport solar simulator. The peak optical power of the solar simulator, measured through an 800 μm diameter aperture, was 750 μW as measured by a Ge detector calibrated at a wavelength of 800 nm. Since the Ge detector responsivity has wavelength dependence, the measured power is only an approximation.

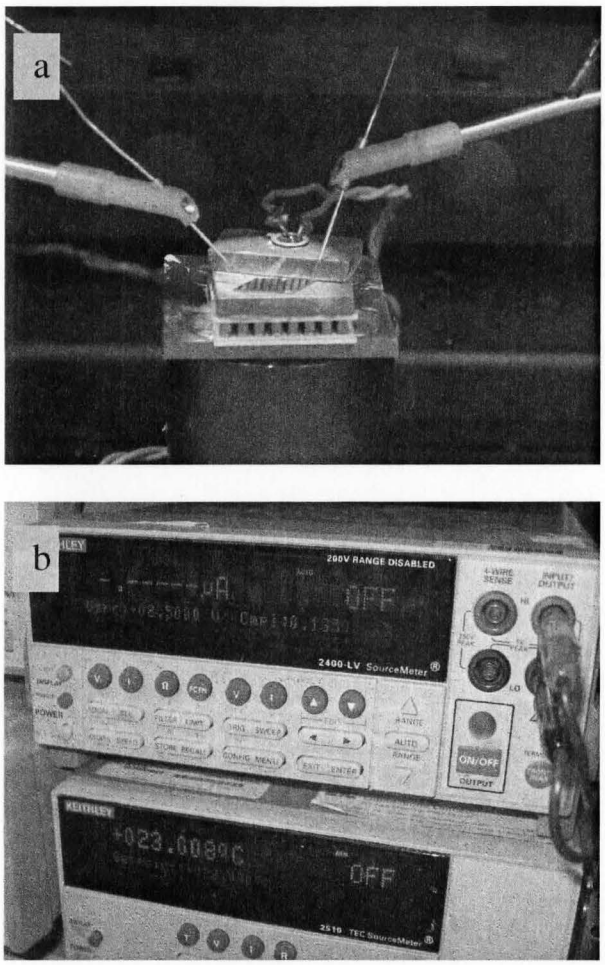

Figure 3.9. (a) The I-V measurement station showing the sample placed on a movable stage with the top and bottom contact probes and light illumination from top. (b) The Keithley 2400 LV source meter.

The measured I-V curves obtained under dark and illuminated conditions with ITO dots are shown in Figure 3.9. A noticeable difference in the current was observed as a result of illumination by the solar simulator.

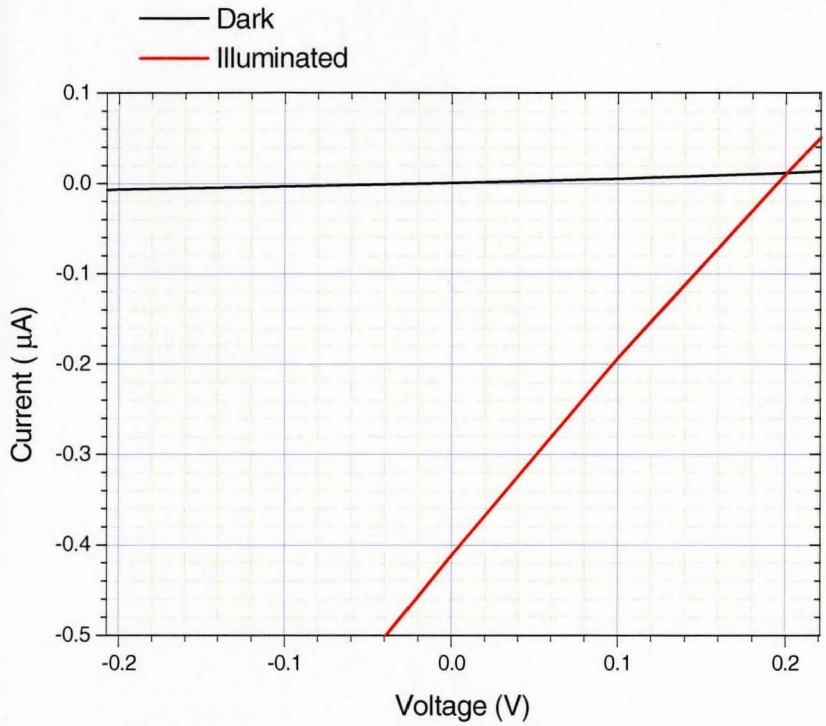

Figure 3.10. I-V results for SU8 2 nanowire solar cell.

As already discussed in chapter 1, the power conversion efficiency, η, of the solar cell is given by:

$$\eta = FF\, I_m V_m / P \qquad \text{Eqn. 1.16}$$

where FF is the fill factor, I_m is the maximum power point, V_m is the maximum voltage point, and P is the incident power. For the I-V results in Figure 3.10, FF~25 %, I_m=1.1 μA, V_m=0.23 V, and P~750 μW and thus η = 0.01 %.

Although this device shows very low conversion efficiency, there are several processing issues that have been identified for improvement. The main issue is the thermal stability of the SU-8 family of resists. As already discussed the resist cannot

withstand high process temperatures. ITO deposited on p-doped GaAs forms a Schottky barrier and has a high sheet resistance. It is critical to reduce this barrier as much as possible. Annealing will reduce, or remove the Schottky barrier, but this step cannot be completed due to the presence of the SU-8 2 which will not withstand the required annealing temperatures.

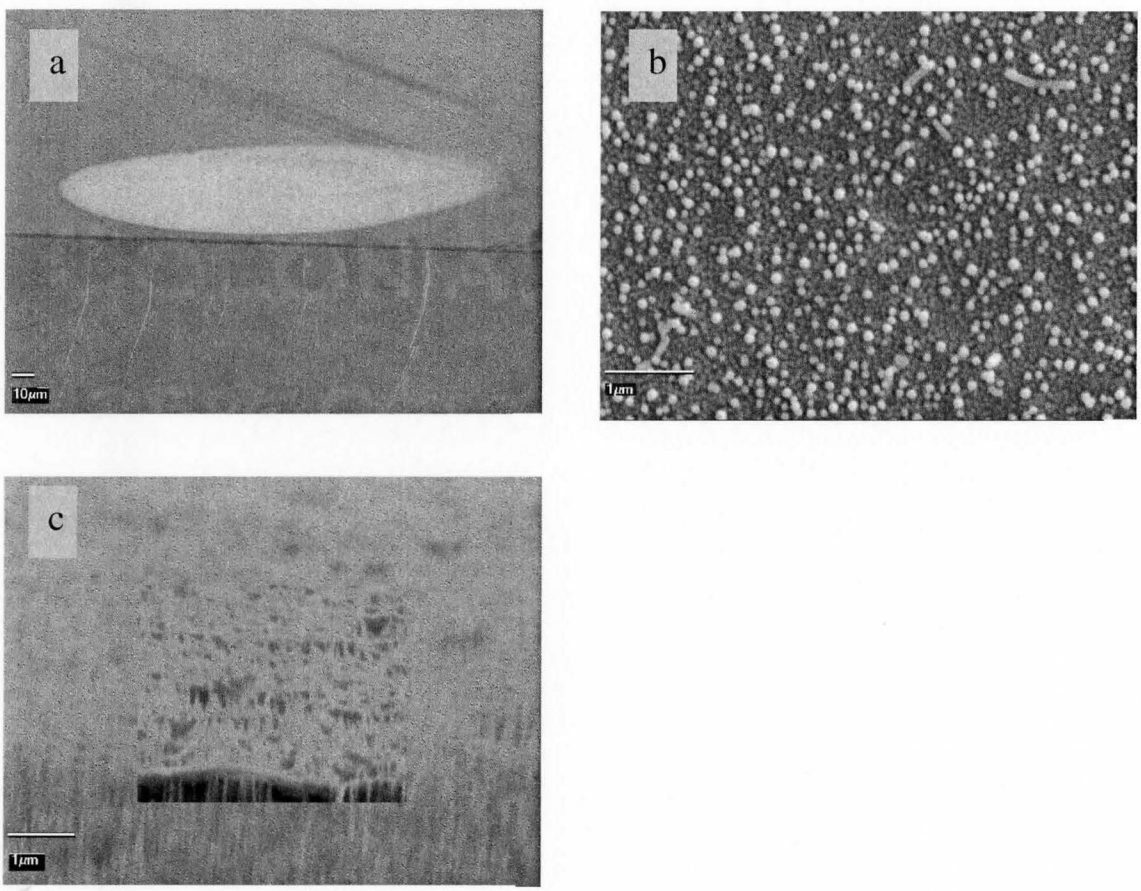

Figure 3.11. SEM images showing the topography of an ITO dot contact. (a) Tilted view of the substrate showing the dot. (b) Top view of the ITO dot. (c) Higher magnification SEM image of a portion of the dot clearly showing ITO is not deposited as a compact film.

Results reported by Kuiqing Peng et al.[3.4] indicated top Ti/Pd/Ag grid electrodes on Si NWs where the contact metals were not deposited as a compact film and hence could lead to a large longitudinal surface resistance. Similarly, the ITO contact on the top surface of our GaAs nanowires did not deposit as a compact film, as seen in SEM images of Figure 3.11 above. Therefore it is clear that the design of the top contact needs to be improved since it could be a contributing factor towards the low efficiency of the device.

Chapter 4: Towards Flexible Solar Cells

This chapter is focused on our attempts to produce flexible solar cells by transferring nanowires (NWs) into flexible substrates.

4.1 Proposed Process for Flexible Solar Cells

The flow diagram of a technique proposed for the fabrication of flexible solar cells using GaAs p-n junction NWs is described. To achieve a flexible solar cell, the process begins with the Gelpak substrate manufactured by the company "Gel-Pak"shown in Figures 4.1 and 4.2(a). Gelpak is a polyester substrate material bonded with a gel film, which according to the manufacturer's definition, is "a highly cross-linked proprietary polymer material".[4.1] For the current research, WF type Gelpak was used which consists of a 5.6 mil gel film bonded to a 6 mil polyester substrate. Optional pressure sensitive adhesive backing was not employed in the current work. The gel film is protected by an easily removable polyethylene sheet.

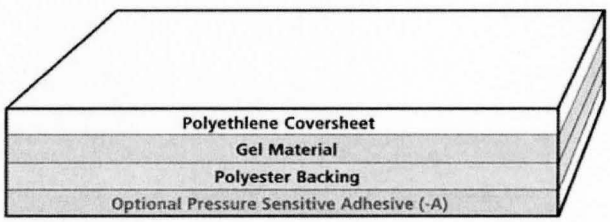

Figure 4.1. Schematic diagram of a WF Gelpak sheet.[4.1]

In the second step (Figure 4.2(b)) a transparent polymer film of SU8 2 is spin-coated on the Gelpak to give a uniform thickness of approximately 2 μm roughly equal to the length of NWs. Subsequently, in Figure 4.2(c), the NWs (still attached to their substrate) are embedded into the polymer film by simple physical contact. To permanently embed the NWs into the polymer film, the polymer is soft baked on a hot plate at 65°C for 1 min and 95 °C for another minute. The baking was followed by removal of the nanowires from their substrate by simple peeling of the Gelpak away from the NW substrate as illustrated in Figure 4.2(d). After peeling, the top of the wires are exposed for electrical contact formation by metallization (Figure 4.2(e)) and another layer of Gelpak is added to the metallized surface for mechanical support (Figure 4.2(f)). This is followed by peeling the previous layer of Gelpak (Figure 4.2(g)) and exposing the other end of wires for bottom metal contact formation (Figure 4.2(h)).

The underlying basis of the above technique lies in the fact that the p-n junction NWs will be removed from their substrate in an upright manner and metallized on their top and bottom for ohmic contacts to be used as a solar cell. Numerous attempts were made to remove the wires from the substrate in the previously described manner and an account of those techniques is given below in separate sections. This part of the thesis is focused on steps a to d of Figure 4.2. Steps e to h were outside the scope of the present thesis.

a. Begin with a thick backing material such as Gelpak

b. Spin-coat a thin layer of polymer

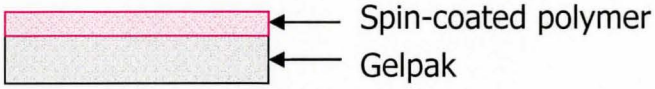

c. Embed the NWs in the polymer

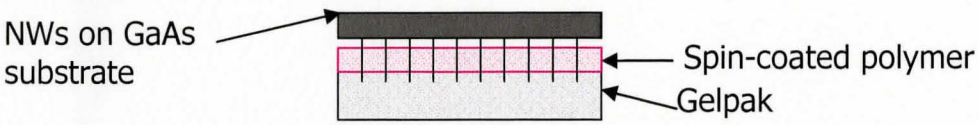

d. Peel away the NWs from the semiconductor substrate

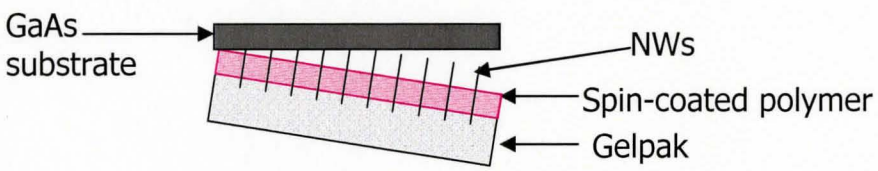

e. Metallize the surface containing the protruding NWs

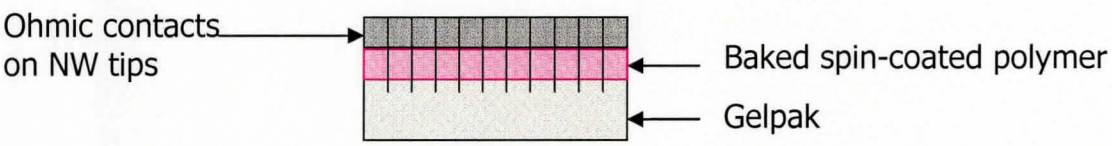

f. Add a second polymer backing to the metallized surface

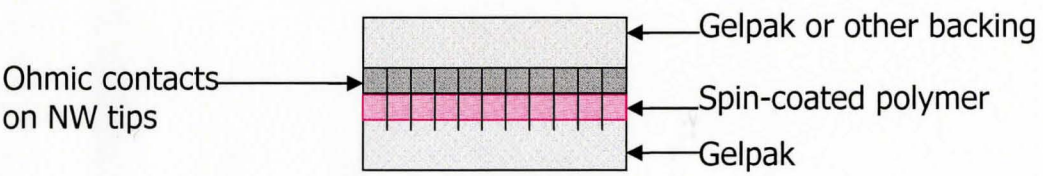

Figure 4.2. Proposed process for producing flexible solar cells as described in the text (continued on next page).

g. Peel away the initial Gelpak backing

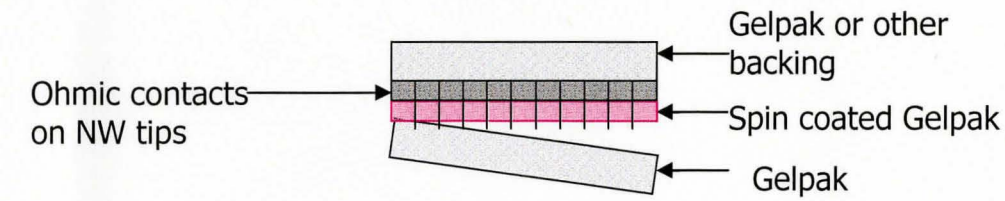

h. Metallize the exposed NW tips

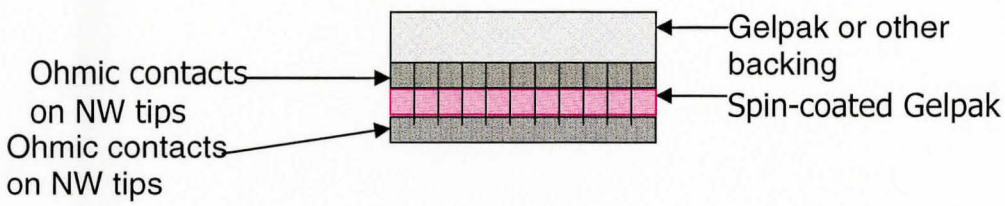

Figure 4.2. (Continued from previous page).[4.2]

4.2 Techniques Employed for Transferring Nanowires onto a Flexible Substrate

The polymers S1818, pf 5070, EGC 1700, SU8 2 and S1827 as summarized in Table 3.1 were used as potential candidates. The research began with an effort to spin a uniform layer of polymer onto a flexible substrate. For this purpose different flexible substrates were investigated including Gelpak, ITO-coated PET (Polyethylene Terephthalate, part number 158531-002 from "Sheldahl") and gold coated PET (part number 2415 from "CP films"). The Gelpak characteristics have already been explained previously. ITO-coated PET and Au-coated PET were investigated with a view to eliminate the bottom contact step later in the process. Both ITO-coated PET and Au-

coated PET have an ITO and Au thickness of 0.06 μm on a PET plastic layer of thickness 635 μm. Each of S1818, pf 5070, EGC 1700, SU8 2 and S1827 were individually spin-coated on Gelpak, ITO-coated PET and Au-coated PET. Subsequently, characterization was done with JEOL JSM-7000F field emission scanning electron microscope (FE-SEM) in the secondary electron mode. The images showed that none of the above polymers could be spun on any of the three substrates to give a uniform layer. In all cases, the polymers failed to wet the whole surface of the substrates and very small surface areas would be left with the polymer in place. Figure 4.3 below illustrates this clearly.

Figure 4.3. SEM image of S1818 spin-coated onto ITO-coated PET. The darker portions are the only places where S1818 has wetted the surface.

The flexible substrates were used in two ways, straight from the manufacturing packaging and also after cleaning. The cleaning was done by dipping the substrate into isopropyl alcohol for 1 min and then running DI water for 1 min following blow-drying with a nitrogen gun. Both clean and unclean samples gave no appreciable differences. However, of the three substrates in use, Gelpak showed more promise in terms of wires

embedding into it. More NWs were seen transferred on the Gelpak surface than the other two substrates. Also, on careful comparison and analysis it was found that SU8 2 wet the Gelpak surface more than the rest of the polymers used.

The focus shifted towards investigating other flexible substrates including Scotch tape, copper tape and carbon tape in addition to the Gelpak already under consideration. The following techniques were investigated to transfer NWs onto a flexible substrate:

1) A peeling method using Gelpak pressed into substrate pieces entirely covered in NWs.
2) A peeling method using Gelpak pressed into small "dot" areas of NWs.
3) A peeling method using carbon tape, copper tape, and Scotch tape.
4) A peeling method using carbon tape supported by a stiff backing.
5) A peeling method using carbon tape in physical contact with Au coated NWs.
6) A "sphere" method.
7) A "probe" method.

Each of these methods is described below.

4.2.1 Gelpak Method

Gelpak was heated to 120 °C for 5 minutes. A GaAs substrate of dimensions roughly around 1 cm x 0.5 cm with GaAs NWs was pressed onto the heated Gelpak such that the NWs were in physical contact with the Gelpak. Various weights were placed on top of the inverted sample starting from 100 g to 2 kg. The weights remained on the sample for 5 minutes. It was found with repeated trials that a weight of 1 kg left on the

sample for 5 min gave the optimum number of detached wires when separated from the sample by simple peeling of the Gelpak away from the substrate, although this maximum number was not really considerable for use in solar cell fabrication. Both the sample and Gelpak were imaged using SEM after detaching.

The SEM images, shown in Figure 4.3, revealed that some NWs did transfer to the Gelpak. However, only about 5% of the wires were removed from the substrate with the majority of wires still remaining on the substrate. Most of the area with removed wires was confined to the edges of the sample, such that an impression of the sample could be seen on the Gelplak with wires along the boundary (as shown in Figure 4.4(a) below). More than 95% of the transferred wires were laying flat against the Gelpak surface. Overall, this process failed to transfer wires in a vertical fashion as desired for the process of Figure 4.2. However, removal of wires by physical contact was shown to be possible.

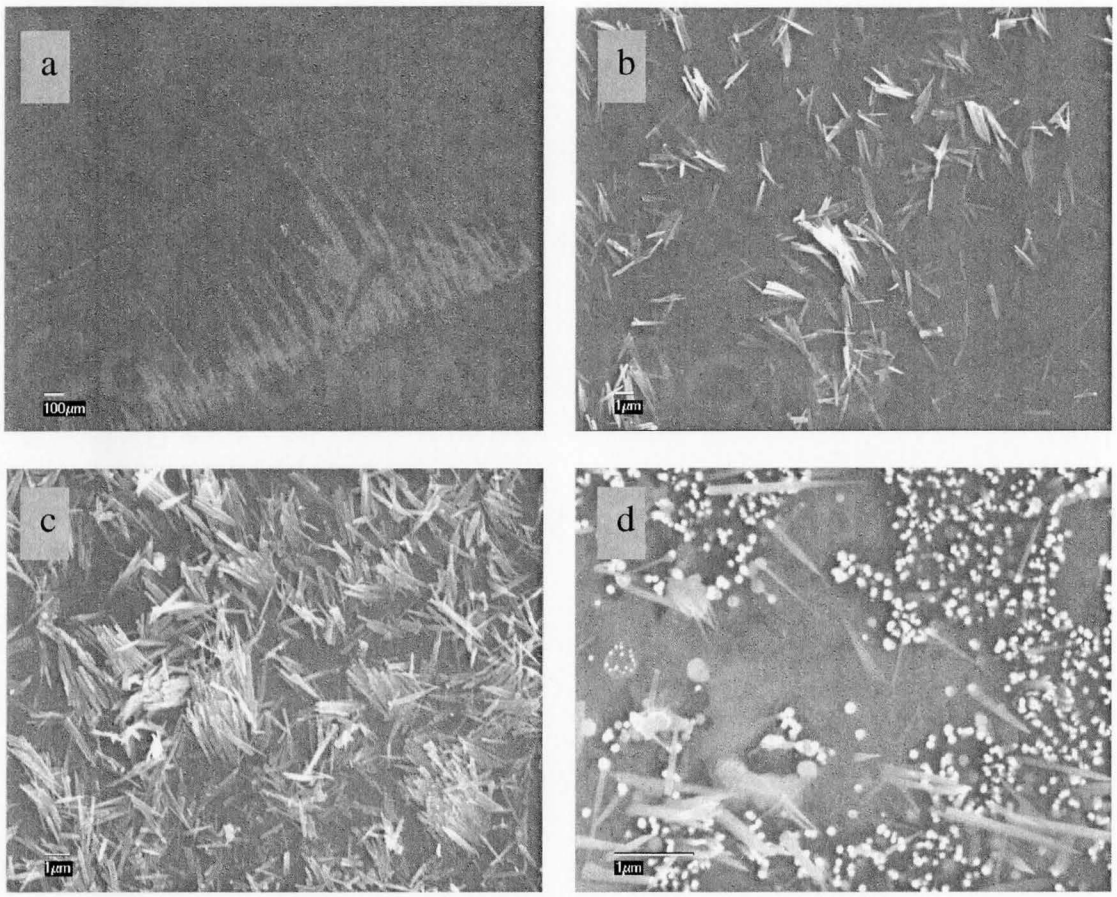

Figure 4.4. Top view SEM images of (a) Gelpak after peeling from the substrate. White lines are the NWs that have been transferred to the Gelpak only along the boundary of the sample. (b) Higher magnification SEM image of Gelpak showing broken wires removed from the substrate. (c) SEM image of broken wires removed from the substrate with higher density. (d) SEM image of the substrate where wires have been removed by peeling away the Gelpak.

4.2.2 Gelpak Method Using Nanowire Dots

Another technique adopted to facilitate removal of wires from the substrate was actually growing the wires in small, localized regions in the form of dots. This was achieved by using a metallic shadow mask to deposit Au in the form of dots with dimensions around 800 μm in diameter and around 200 μm apart. These Au dots were

subsequently used for NW growth so that wires grew only in the regions of the Au dots with the surrounding area of the substrate free of wires. This method facilitated removal of the wires by minimizing the peeling area; that is, the peeling of a localized dot of NWs would be comparatively much easier than a large surface area completely covered in thickly populated wires.

Gelpak was again used to remove the NW dots. The Gelpak was heated to 120 °C for 5 minutes to soften the Gelpak and facilitate NW transfer. The substrate with NW dots was inverted onto the sample and different pressures were applied on the sample with weights ranging from 100 g to 2 kg.

SEM images of the Gelpak and the substrate after separation by peeling showed that most of the wires remained intact on the substrate, with only a tiny fraction being removed. However, the density of the removed wires was much greater than that obtained by the previous method. Most of the NWs were confined to the dot circumference, and were broken and lying down randomly.

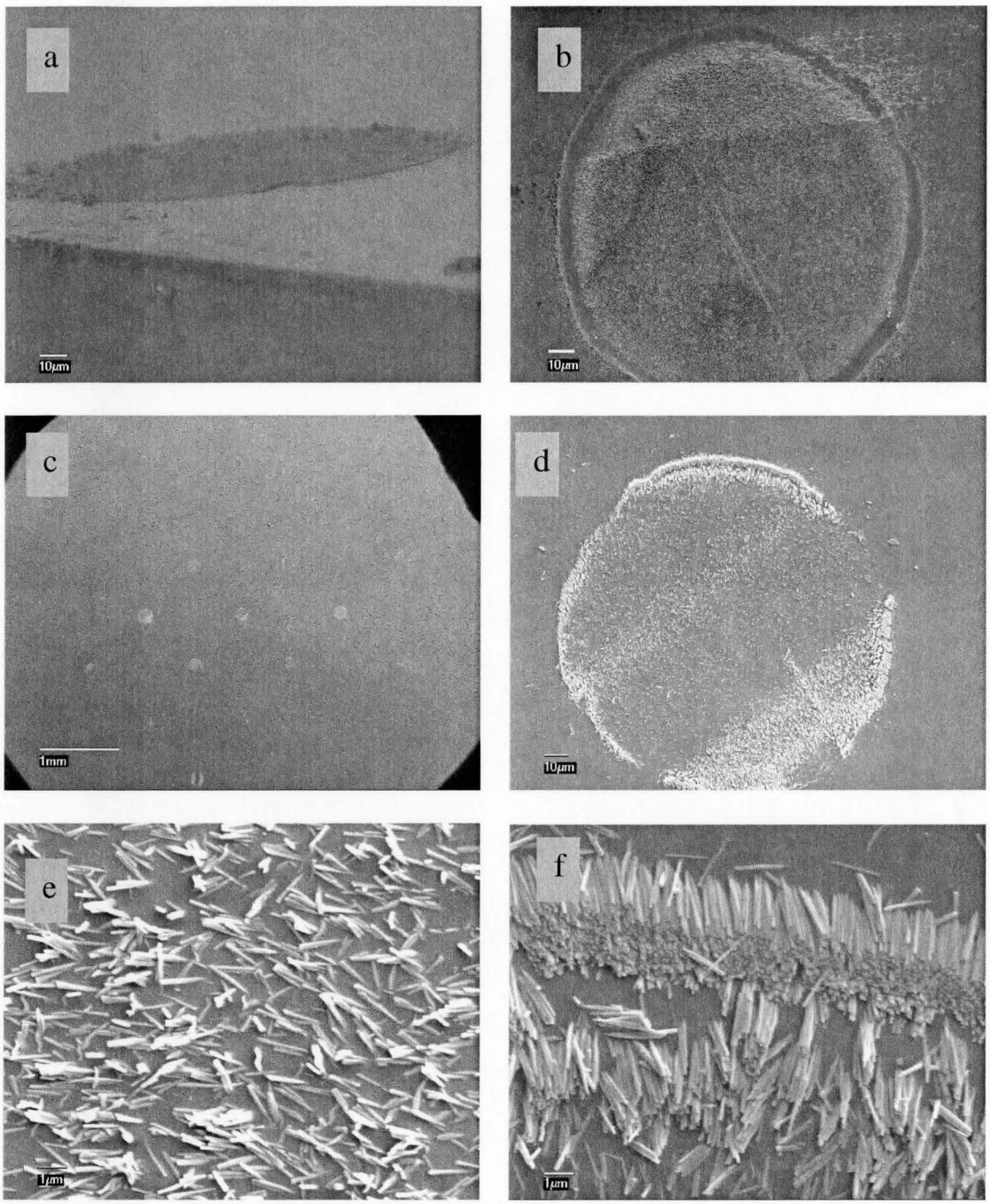

Figure 4.5. SEM images of nanowire dots. (a) Substrate with NWs grown as dots. (b) Top view of substrate showing NWs after Gelpak peeling. (c) Top view of Gelpak showing NWs transferred after peeling from substrate. (d) Gelpak showing wires transferred from an individual dot. (e) Top view showing broken wires laying flat on the Gelpak after peeling. (f) SEM image showing a dense population of wires laying flat along the edge of the dot.

4.2.3 Removal of Nanowires by Tape

Removal of NWs from their substrate was also attempted by physical contact with various adhesive tapes, including carbon tape, copper tape, and two different types of Scotch tape. Carbon tape part number 5072 was supplied by "Structure Probe Inc, SPI Supplies", while copper tape and both Scotch tapes were supplied by 3M (Highland 897 Ruben/Cinta from 3M with stripes along the longitudinal side and Scotch Transparent Tape 600, 1 inch core).

The NW peeling process was performed by four different methods for each of the three tapes:

(1) The tape was placed on the substrate followed by immediate removal;

(2) The tape was placed on the substrate and different weights, ranging from 50 g to 2 kg were placed on the tape for 30 minutes before peeling;

(3) The tape was placed on the substrate and left for 24 hrs to allow for curing of the adhesive;

(4) The tape was placed on the substrate and weights were placed on the tape for 24 hrs to allow for curing of the adhesive.

Again, SEM JOEL 7000F was used to characterize the peeling process. First, the carbon tape would stretch and either get clumped or would tear upon peeling. Although some regions of the peeled carbon tape showed clusters of wires, the wires were lying down in random directions on the carbon tape and not all regions of the tape exhibited NWs. Figure 4.5 shows the carbon tape process.

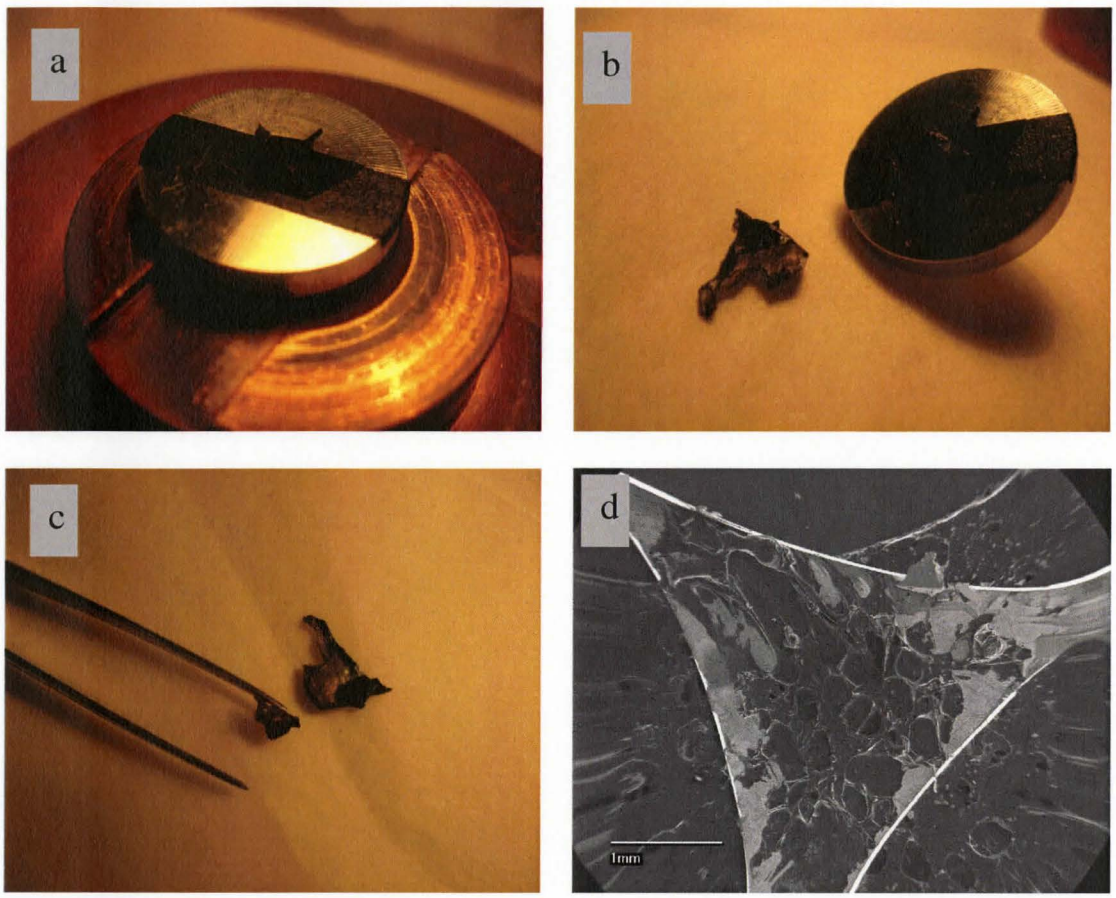

Figure 4.6. Continued on next page.

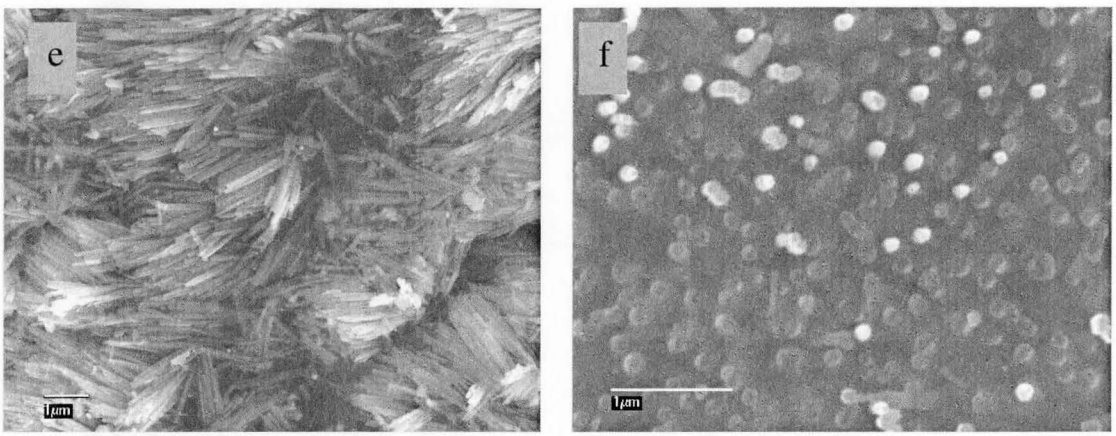

Figure 4.6. (a) Peeling process through carbon tape. Stub with double-sided carbon tape and sample mounted on it facing up. The clumping and stretched part of carbon tape after peeling can be seen sitting on the substrate. (b) Image of the stub with substrate and left over part of tape after peeling. (c) Peeled part of the tape and clumped part of the tape tweezed off from the substrate for SEM imaging. (d) SEM image of a triangular NW sample after removal of carbon tape. The black portion shows the carbon tape still adhering to the substrate after removal. (e) A portion of carbon tape after peeling showing clusters of NWs. (f) Top view SEM image of the substrate where wires have been removed by carbon tape, showing NW "stumps" remaining on the substrate.

SEM images of the copper tape and both types of Scotch tape after peeling off from the substrate showed comparatively thinner population of NWs scattered and lying down. Figure 4.6 shows the comparison of the three tapes. One common observation about all three tapes was that they left a residue on the NW sample that would render the sample unfit for further use.

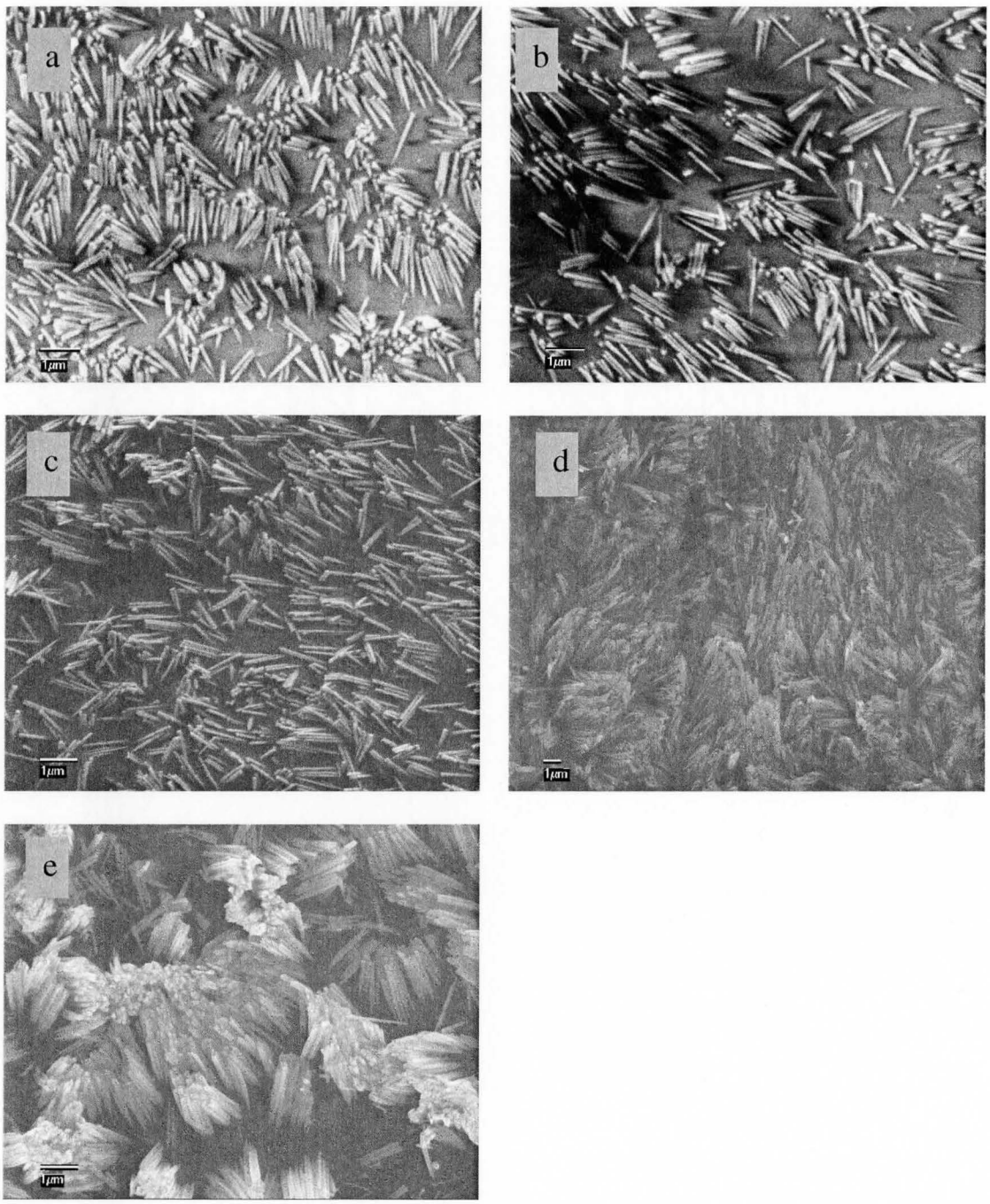

Figure 4.7 (a) SEM image of 3M regular scotch tape after peeling off from substrate. (b) SEM image of Cu tape after peeling off from substrate (c) SEM image of 3M Highland tape after peeling off (d, e) SEM image of carbon tape after peeling off from substrate for comparison

These results suggested that of the four types of tapes used, carbon tape could be more successful in removing NWs from the substrate since it showed thicker population of wires in clusters when imaged by SEM. This gave way to another option for investigation, whether supporting the carbon tape on a stiff backing before peeling could reduce its tendency to stretch and clump.

4.2.4 Removal of Nanowires by Tape with Stiff Backing

Based on the findings of the previous section, the carbon tape was supported by a stiff backing and then applied to the substrate. For this purpose the Al stub part number 01506-BA from "SPI Supplies" used for mounting the samples into the JOEL 7000F SEM was used as a stiff backing. The double-sided carbon tape of the same length as the diameter of stub was placed on it. Parallel to this another stub with double sided carbon tape and the NW sample of area roughly ~1cm^2 mounted on it facing upwards was prepared. The first stub was brought in contact with the second stub, and then pulled away in a peeling manner, with the aim that the tape would peel NWs away from the substrate over its whole area. However, it was found that the carbon tape bonded more strongly to the substrate than to the stiff backing material, the stub in this case. In the peeling process the tape would come off the stub and adhered to the NW sample . As a result, it was not easily removed from the substrate. Repeated trials with increasing and decreasing the size of the NW sample keeping the carbon tape size constant proved the same result. SEM images in Figure 4.7 of the portions of carbon tape that were removed

showed clusters of wires lying in random directions similar to the previous results without stiff backing.

In order for the sample to hold onto the stub strongly, silver paste was also tried instead of carbon tape. The paste was applied on the bottom of the sample as well as the stub before sticking them together and also on the four corners of the sample after it was adhered to the stub. However, when the carbon tape was applied with the stiff backing and peeled off, the sample either broke away from the stub and stuck to the tape or the tape stuck to the sample as in the previous experiments and had to be removed by peeling off with tweezers which resulted in its clumping and stretching, again rendering it unfit for use as a flexible substrate.

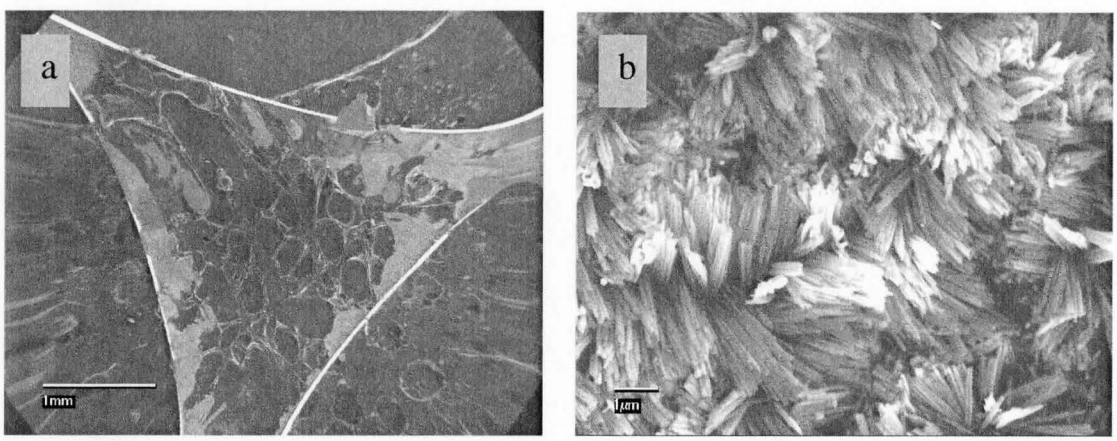

Figure 4.8. (a) SEM image showing a triangular substrate after carbon tape with stiff backing was used to peel off NWs. The dark portion is the carbon tape left behind on the substrate while the lighter portion shows the area where NWs were removed. (b) SEM image of the carbon tape after it was removed from the substrate. Clusters of wires in all directions can be seen.

Alternately, a sample was prepared like that shown in Figure 3.6. Working on the idea that the spun-on polymer would support the NWs and keep them straight after

removal, carbon tape was again applied to the sample and then peeled off. It was found that the polymer SU8 2 made it practically impossible for the NWs to detach from the substrate. The tape adhesive could not bond with the polymerized surface of the sample and hence no wires were removed at all by peeling the surface off with carbon tape.

4.2.5 Removal of Au-Coated Nanowires by Tape

Another technique adopted to facilitate the removal of NWs from their substrate onto the tape by peeling included deposition of a Au layer on top of the wires. It was hoped that the Au layer would act as a support layer to facilitate peeling of the NWs over larger areas. It was expected that the Au layer would offer a smooth surface for removal by peeling with tape as well as form an ohmic contact. The Au deposition was attempted with thickness ranging from 100 nm to 700 nm deposited by electron beam evaporation. The Au was deposited directly on the sample as well as after tilting the sample by 45 degrees, so as to isolate the Au deposition to the top of the NWs. SEM images in Figure 4.8 of the Au coated NWs showed that the Au did not deposit as a smooth layer, but was deposited preferentially on top of the wires.

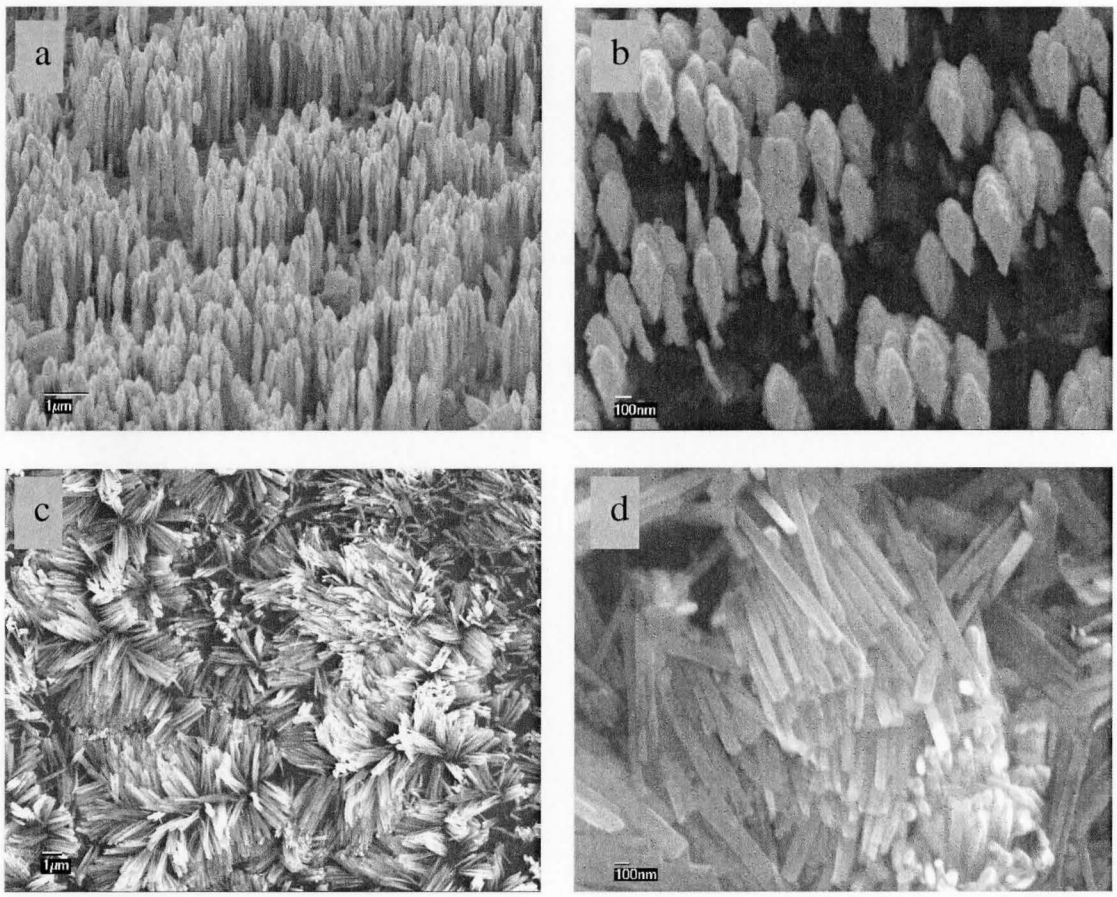

Figure 4.9. SEM images of (a) NWs covered by 600 nm of Au, and (b) NWs covered with 700 nm of Au deposited by e-beam evaporation on samples tilted by 45°. (c, d) Carbon tape after peeling from NW sample with Au covered wires.

4.3 The Sphere Method

The "sphere method" entailed the use of solder spheres from "Qualitek International Inc." (part number: SS/SN63/020/50K) with a diameter of ~500μm. The spheres were mounted rigidly on a plane, horizontal surface in a hexagonal close-packed arrangement using double-sided tape. A Gelpak film was heated on a hot plate to 120 °C for 5 minutes in order to soften the gel and placed onto the spheres so that the silicone

surface of the gel faced up. The NWs were pressed into the Gelpak using a wt ~ 1 kg. After 5 minutes, the weight was removed and Gelpak was separated from the substrate.

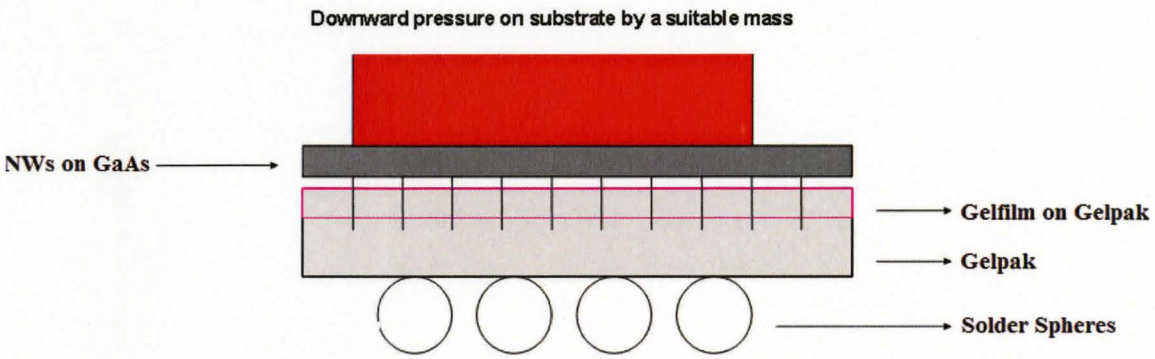

Figure 4.10. Illustration of the "sphere method".

SEM images of the substrate and Gelpak in Figure 4.8 showed successful transfer of NWs from the substrate into the Gelpak in the form of dots comparable to the contact area of the spheres.

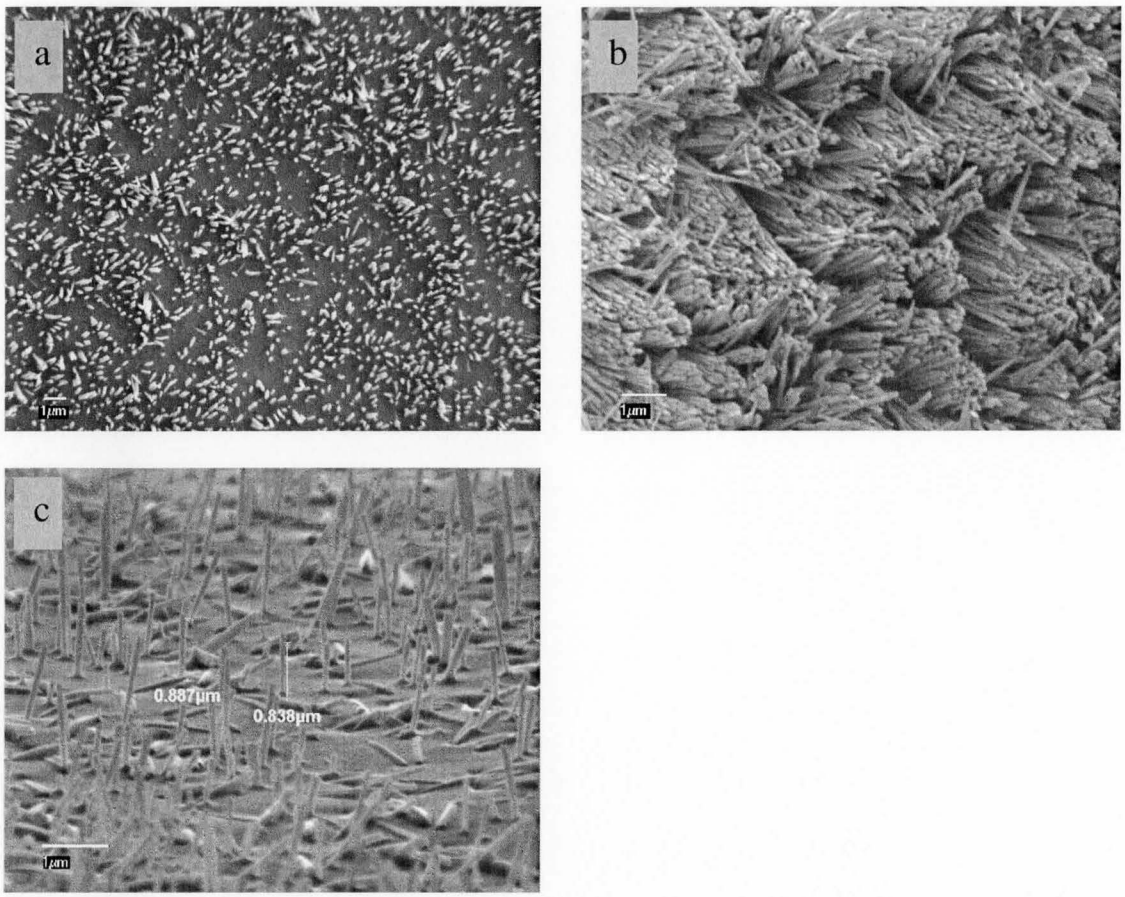

Figure 4.11. (a) Top view SEM image of the Gelpak with NWs embedded in an upright orientation. (b) Higher magnification SEM image of NWs transferred onto the Gelpak. (c) Tilted SEM view of the NWs transferred onto Gelpak. The wires can be seen standing erect.

4.4 The Probe Method

This method, illustrated in Figure 4.12, is similar to the sphere method described in the previous section. The NW substrate was placed flat on a plane horizontal surface with NWs facing up. Gelpak was heated to 120 ˚C for 5 minutes and placed on top of the wire sample with the silicone layer pressing against the NWs. A probe consisting of a simple ball point pen with tip size comparable to that of the spheres in the previous

section were manually pressed into the Gelpak. Subsequently, the Gelpak was removed from the NW substrate.

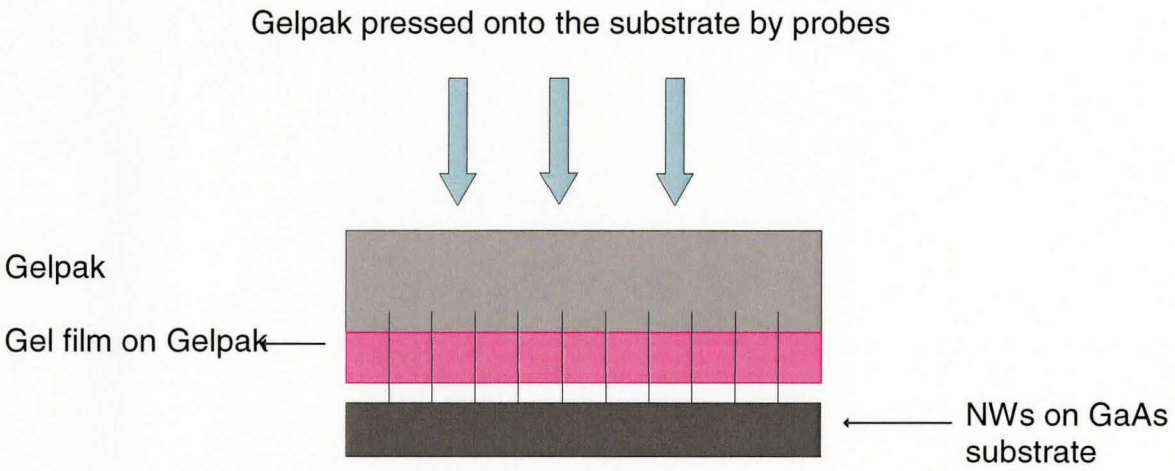

Figure 4.12. Schematic diagram of the probe method.

SEM images in Figure 4.12 showed the success of this method similar to the sphere method. The wires were successfully transferred onto the Gelpak in the form of dots with clusters of wires embedded vertically.

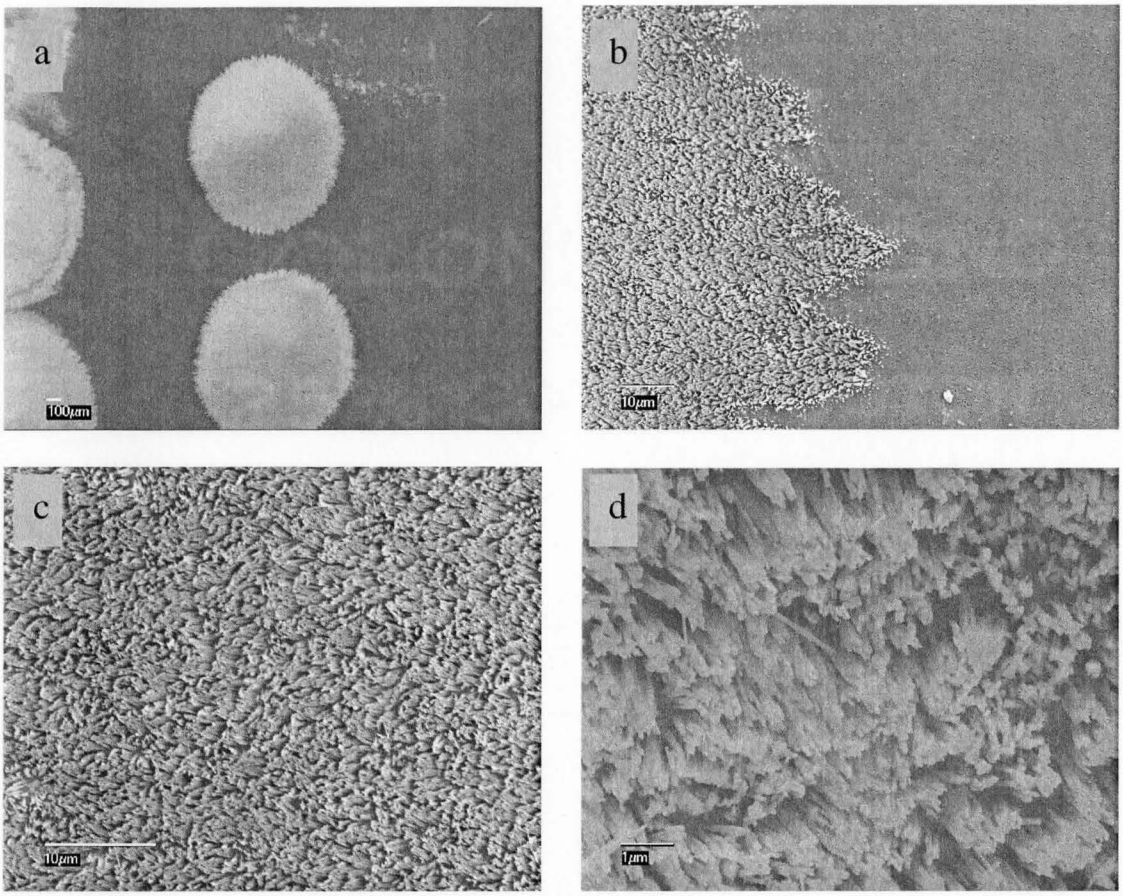

Figure 4.13. (a) SEM image of the Gelpak showing dots of wires removed after using the probe method. (b) High magnification SEM image of edge of the dot on Gelpak with removed wires. (c) Top view SEM image of the NWs removed from the substrate by the probe method. The wires can be seen standing erect. (d) High magnification SEM image of the NWs removed from the substrate onto Gelpak by the probe method.

After the NWs were transferred by repeated trials through the sphere method and the pen tip method, confirming the success of both the methods, the Gelpak sample with the transferred nanowires was spin-coated with SU8 2 under similar conditions as in Chapter 3 where the NWs were investigated for use as solar cells, ie 4500 rpm for 60 s. The sample was also soft-baked as previously done, by placing it on a covered hot plate for 1 min at 60 °C and 1 min at 95 °C. Gelpak can withstand temperatures up to 220°C as

per the manufacturer's specifications. This was followed by RIE using oxygen plasma with the same conditions as in our previous experiment. Figure 4.14 shows SEM images of the process. These wires are now ready for top contacting as part of the solar cell fabrication process.

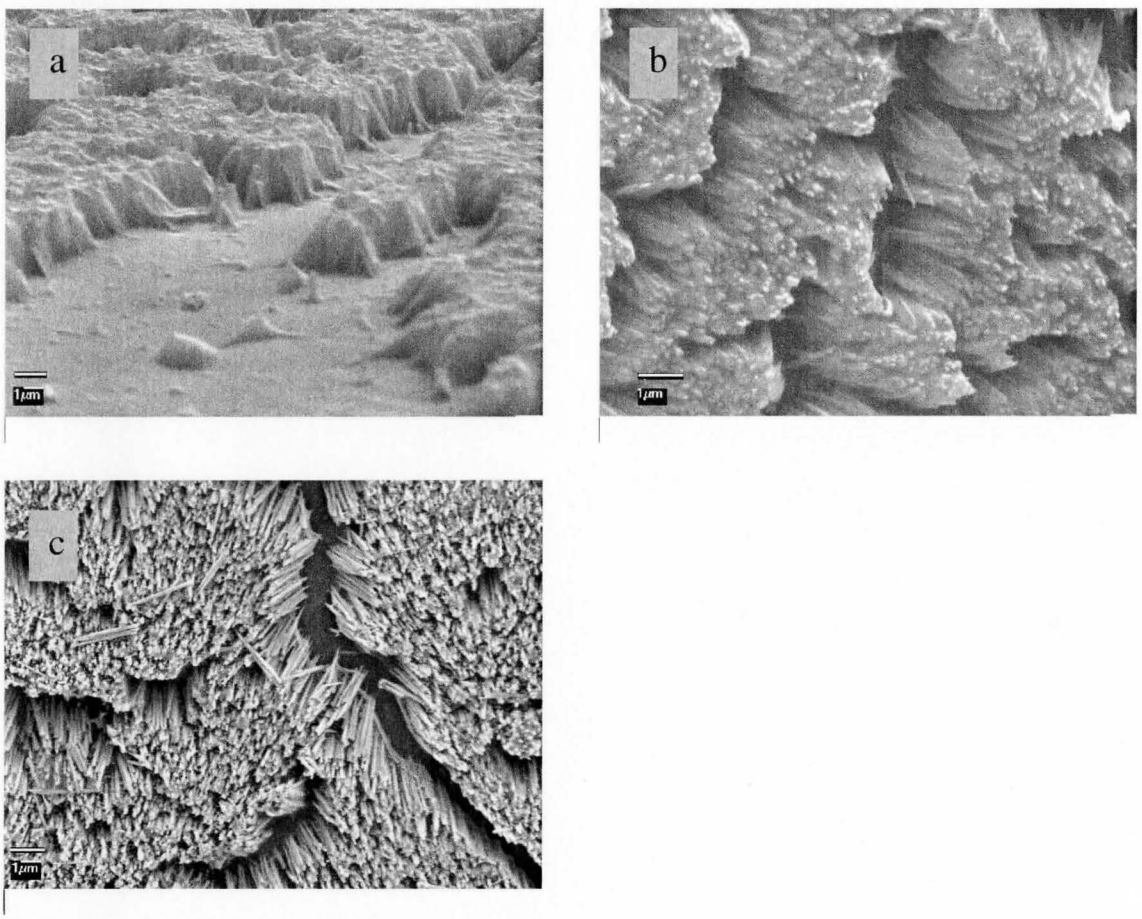

Figure 4.14. SEM images showing NWs transferred successfully onto Gelpak by using the probe method and spin coated with SU8 2, followed by reactive ion etching. (a) Tilted view of the Gelpak sample showing NWs after spin coating with SU8 2 at 4500 rpm for 60 s. (b) Top view image of the transferred NWs with SU8 2. (c) Top view of the same sample of NWs after reactive ion etching.

Chapter 5: Conclusions and Future Work

As a first part of this thesis, the potential of core-shell GaAs p-n junction nanowires as solar cells was investigated by following the steps outlined below:

1) Growth of core-shell GaAs p-n junction nanowires on an n-type GaAs (111)B substrate through the VLS method, using gas source molecular beam epitaxy.
2) Metallizing the bottom side of the substrate using electron beam evaporation for bottom contact using standard n-type contact metals: 250Å Ni, 500 Å Ge and 1200 Å Au.
3) Annealing the bottom contact with capping using rapid thermal annealing for 30 s at 380 °C in an atmosphere of nitrogen gas.
4) Supporting the NWs by spinning a transparent polymer (SU8 2 from MicroChem) onto the substrate with the conditions that it would give a uniform layer close to the height of the NWs, which in this case was ~2-2.5 μm.
5) Etching back the polymer by reactive ion etching using oxygen plasma to expose the top of the wires for contacting purpose.
6) Sputter deposition onto the top of the exposed wires with ~400 nm indium tin oxide for contacting in the form of dots using a mask with hole sizes ~800 μm in diameter and ~200 μm apart.
7) I-V measurements performed by using a highly stable DC power source and digital multimeter, applying voltages between +10V and -10V, under dark and

illumination conditions using a solar simulator with the peak optical power of the solar simulator, measured through an 800 μm diameter aperture, of 750 μW.

8) Characteristic curves of a typical p-n junction observed with a sharp difference in current after illumination by the solar simulator, confirming that the device behaved as solar cell. The I-V results show that the device fabricated has an efficiency η of 0.01%, with fill factor~25 %, maximum current point I_m=1.1 μA and maximum voltage point V_m=0.23 V.

As a second part of this thesis, a fabrication technique towards making a flexible solar cell was investigated based on the fact that the p-n junction nanowires can be transferred onto a flexible substrate standing straight in the same way they grow on the substrate itself. The idea was to get them transferred onto the flexible substrate and then follow the same technique as mentioned above to get them working as a solar cell.

The most successful method was the sphere method, wherein solid solder spheres with diameter of ~500μm were mounted rigidly on a plane horizontal surface in a hexagonal close-packed arrangement using double-sided tape. A Gelpak film was heated on a hot plate to 120 °C for 5 minutes in order to soften the gel and placed onto the spheres so that the silicone surface of the gel faced up. The NWs were pressed into the Gelpak using a 1 kg weight. After 5 minutes, the weight was removed and Gelpak separated from the substrate. SEM images of the substrate and Gelpak showed successful transfer of NWs from the substrate into the Gelpak in the form of dots comparable to the contact area of the spheres.

The probe method was similar to the sphere method described in the previous section. The NW substrate was placed flat on a plane horizontal surface with NWs facing up. Gelpak was heated to 120 °C for 5 minutes and placed on top of the wire sample with the silicone layer pressing against the NWs. A probe consisting of a simple ball point pen with tip size comparable to that of the spheres in the previous section were manually pressed into the Gelpak. Subsequently, the Gelpak was removed from the NW substrate. SEM images showed the success of this method similar to the sphere method. The wires were successfully transferred onto the Gelpak in the form of dots with clusters of wires embedded vertically.

The research conducted in this thesis is basically focused on the fabrication techniques, and mainly on NWs transfer onto a flexible substrate. Also, the potential of GaAs p-n junction NWs as solar cells was also investigated as a major part of the thesis. However, the work done is at a very preliminary and early stage and much needs to be done in this regard to develop it into an inexpensive, easily manufacturable and reproducible process.

There are two main issues that need to be investigated in the development of solar cells based on nanowires in this research: i) the design of the process flow, and ii) the design of the nanowire material structure. In the first part of the research where NWs have been investigated as functioning solar cells, there are several processing issues that have been identified for improvement that can affect the efficiency of the device. The main issue is the thermal stability of the SU-8 family of resists. The resist cannot withstand high process temperatures. For example, at 300-315 °C, the SU-8 will

experience 5% weight loss. ITO deposited on p-doped GaAs forms a Schottky barrier and has a high sheet resistance. Annealing will reduce, or remove the Schottky barrier, but this step cannot be completed due to the presence of the SU-8 which will not withstand the required annealing temperatures. As a result, the SU-8 cannot be annealed to temperatures appropriate for alloying metal contacts. Hence the possibility of replacing SU8 2 by a transparent polymer with higher thermal tolerance can be investigated.

Also changing the thickness of ITO for top contact material as well as investigating other materials for top contact can be initiated. The p-n junction in the NWs or the Schottky barrier between top contact ITO and the p-type material on top of the NWs needs to be investigated as well. This could be done by comparing the I-V curves of n-type GaAs NWs and p-type GaAs NWs grown and processed under exactly the same conditions as the p-n junction GaAs NWs grown and processed for the current research.

In the area of transferring NWs, a few techniques can be investigated. Firstly, in the probe method which has given the best results so far, and is also reproducible, a standard pressure technique needs to be developed, which in the current research has been limited to a manual pressure.

References

[1.1] Energy Sciences Workshop and Technical Reports, BES Workshop Report on "Solar Energy Utilization", April 18–21, 2005 (www.sc.doe.gov-Basic).

[1.2] B. Tian, X. Zheng, T. J. Kempa, Y. Fang, N. Yu, G. Yu, J. Huang, and C. M. Lieber "Coaxial Silicon Nanowires as Solar Cells and Nanoelectronic Power Sources", Nature 449 (2007) 885-889.

[1.3] http://www.scinece.nasa.govt/headlines/y2002/solarcells.html

[1.4] M. Law, L.E. Greene, J.C. Johnson, R. Saykally, and P. Yang, "Nanowire Dye-Sensitized Solar Cells", Nat. Mat. 4 (2005) 455-459.

[1.5] P. Yang, "Nanowires Increase Electron Conduction 100-Fold in Solar Cell", Report for Materials Science Division, Berkeley Lab, Dept. of Energy, USA (www.lbl.gov/~msd/Pls/Yang/06/04_Yang_nanowire_solar.pdf).

[1.6] W.T. Welford and R. Winston, *The Optics of Non-Imaging Concentrators* (Academic Press, 1998).

[1.7] http://scinece.nasa.govt/headlines/y2002/solarcells.html

[1.8] http://www.udel.edu/igert/pvcdrom/index.html

[1.9] http://www.springerlink.com/content/cb4v3junpqcgnwr9/fulltext.pdf

[1.10] J. Nelson, *The Physics of Solar Cells* (Imperial College Press, 2002).

[1.11] S.O. Kasap, *Principles of Electrical Engineering Materials and Devices,* 2nd ed. (McGraw Hill, USA, 2002).

[1.12] T. A. Yates, "Solar Cells in Concentrating Systems and Their High Temperature Limitations", University of California, Santa Cruz 2003, (http://quantum.soe.ucsc.edu/research/SolarCell/Tarn_Senior%20Thesis.pdf).

[1.13] B. Streetman and S.K. Bannerji, *Solid State Electronic Devices*, 6th ed. (Prentice Hall, 2006).

[1.14] http://www.rpi.edu/dept/pys/Courses/PHYS1010/Persans.pdf

[1.15] http://www1.eere.energy.gov/solar/absorption_conduction.html

[1.16] P. Wurfel, *Physics of Solar Cells: From Principles to New Concepts* (Wiley, 2005).

[2.1] Newport Corporation: www.newport.com

[2.2] A. Cho, P.Y. Smith, and J.F. Smith, "Film Deposition by Molecular Beam Techniques", J. Vac. Sci. Technol. 8 (1971) S31-S38.

[2.3] A. Cho and J. Arthur, "Molecular Beam Epitaxy", Prog. Solid-State Chem. 10 (1975) 157-192.

[2.4] http://projects.ece.utexas.edu/ece/mrc/groups/street_mbe/mbechapter.html

[2.5] M.A Herman and H Sitter, *Molecular Beam Epitaxy*, 2nd ed. (Springer-Verlag, Germany, 1996).

[2.6] http://www-opto.e-technik.uni-ulm.de/forschung/jahresbericht/2002/ar2002_fr.pdf

[2.7]http://www.veeco.com/products/Epitaxial_Equipment/MBE_Components/PID_Temperature_Controllers

[2.8] Private communication, R.R. LaPierre, McMaster University.

[2.9] A.P. Levitt, *Whisker Technology* (Wiley Interscience, 1970) pp. 47-69.

[2.10] E.S. Greiner, J.A. Gutowski, and W.C. Ellis, "Preparation of Silicon Ribbons", J. Appl. Phys. 32 (1961) 2489-2490.

[2.11] Y. Wu and P. Yang, "Direct Observation of VLS Nanogrowth", J. Am. Chem. Soc. 123 (2001) 3165-3166.

[2.12] G.A. Bootsma and H.J. Gassen, "A Quantitative Study on the Growth of Silicon Whiskers from Silane and Germanium Whiskers from Germane", J. Cryst. Growth 10 (1971) 223–234.

[2.13] M.C Plante and R.R. LaPierre, "Growth Mechanisms of GaAs Nanowires by Gas Source Molecular Beam Epitaxy", J. Cryst. Growth 286 (2006) 394-399.

[2.14] Purdue University, Radiological and Environmental Management Dept. (http://www.ipfw.edu).

[2.15] http://www.nrel.gov/pv/measurements/scanning_electron.html

[2.16] http://mse.iastate.edu/microscopy/beaminteractions.html

[2.17]http://www.elettra.trieste.it/experiments/beamlines/lilit/htdocs/people/luca/tesihtml/node28.html#sec:plasma

[2.18] http://acept.asu.edu/PiN/rdg/elmicr/elmicr.shtml

[2.19] Centre for Emerging Device Technologies, McMaster University (http://www.eng.mcmaster.ca).

[2.20] https://www.memsnet.org/mems/processes/etch.html

[2.21] http://www.nd.edu/~ndnf/processing/PE2400.html

[2.22] http://www.espi-metals.com/tech/sputtering.pdf

[2.23] http://www.cryosem.com/Manuals/Current_Technical_Briefs/TB-SPUTTER.pdf

[2.24] http://cnx.org/content/m11369/latest

[2.25] http ://www.mdcvacuum.com/searchs/doc/ThinFilmDep-Intro.html

[2.26] http://www.icmm.csic.es/fis/english/evaporacion_electrones.html

[3.1] R. LaPierre and J. Czaban, internal report, Nanowire Solar Cell Research and Development Project, Quarterly Report, March 28, 2008, McMaster University, Department of Engineering Physics.

[3.2] http://www.microchem.com

[3.3] http://www.microchem.com/products/pdf/SU8_50-100.pdf

[3.4] K. Peng, Y. Xu, Y. Wu, Y. Yan, S.T. Lee, and J. Zhu, "Aligned Single-Crystalline Si Nanowire Arrays for Photovoltaic Applications" , Small 1 (2005) 1062-1067.

[4.1] http://www.Gelpak.com

[4.2] S. Sheyma, Internal Report for Ray LaPierre, Summer, 2005, McMaster University, Department of Engineering Physics.